Numerical investigation of von-Kármán flows involving non-Newtonian fluids

by

Maria Tabassum

A thesis submitted in partial fulfillment of the requirements
for the degree of Master of Science in Mathematics

Supervised by

Dr. Meraj Mustafa Hashmi

School of Natural Sciences,
National University of Sciences and Technology,
Islamabad, Pakistan

2018

FORM TH-4

National University of Sciences & Technology

MS THESIS WORK

We hereby recommend that the dissertation prepared under our supervision by: Maria Tabassum, Regn No. 00000172914 Titled: Numerical Investigation of von-Karman flows involving non –Newtonian fluids be accepted in partial fulfillment of the requirements for the award of **MS** degree.

Examination Committee Members

1. Name: Mujeeb Ur Rehman Signature: _____

2. Name: Dr. Ammar Mushtaq Signature: _____

External Examiner: Dr. Nasir Ali Signature: _____

Supervisor's Name: Dr. Meraj Mustafa Hashmi Signature: _____

_____ 09/08/18

Head of Department Date

COUNTERSINGED

Date: 09/08/18 **Dean/Principal**

THESIS ACCEPTANCE CERTIFICATE

Certified that final copy of MS thesis written by **Maria Tabassum**, (Registration No. **00000172914**), of **School of Natural Sciences** has been vetted by undersigned, found complete in all respects as per NUST statutes/regulations, is free of plagiarism, errors, and mistakes and is accepted as partial fulfillment for award of MS/M.Phil degree. It is further certified that necessary amendments as pointed out by GEC members and external examiner of the scholar have also been incorporated in the said thesis.

Signature: _____

Name of Supervisor: Dr. Meraj Mustafa Hashmi

Date: 09/08/18

Signature (HoD): _____

Date: 09/08/18

Signature (Dean/Principal): _____

Date: 09/08/18

THIS DISSERTATION IS DEDICATED TO

MY LOVING PARENTS

FOR THEIR ENDLESS LOVE,

PRAYERS AND SUPPORT.

Acknowledgement

In the name of almighty Allah, the merciful, the beneficent, all praises (belong) to Allah alone, the cherisher and sustainer of the world.

I deem it a great honor to express my deepest sense of gratitude to my honorable and esteemed supervisor Dr. Meraj Mustafa Hashmi for his continuous support throughout my research, for his patience, motivation, enthusiasm, and immense knowledge. His guidance helped me in all the time of research and writing of this thesis. His insistence for excellence kept me focused and well-directed. His pleasant and committed nature along with energetic endorsement was a source of spirit for me to complete this thesis.

My sincere gratitude is to my GEC members, Dr. Ammar Mushtaq (RCMS) NUST and Dr. Mujeeb ur Rehman (SNS) NUST, for their guidance and support that helped me in completing this thesis in time.

This acknowledgement would be incomplete unless I offer my humble veneration to my loving parents, Mr. Munawar Hussain and Mrs. Nayer Sultana for their great efforts, support and encouragement during the period of this work. I would extend my gratitude to my brothers for their support during my thesis.

I would also like to thank my friends who helped and support me throughout the MS duration.

Maria Tabassum

Contents

Abstract

The steady state laminar flow induced over a disk rotating with uniform angular velocity about the vertical axis is a well-known fluid dynamics problem that has practical importance. Such problem is apparent in a number of technical applications dealing with electrochemical systems, deposition of coatings on surfaces, rotor- stator system, viscometers and many others. Despite the fact that almost all industrial fluids are non-Newtonian, von-Kármán's analysis for non-Newtonian fluids has been scarcely attempted.

We have formulated and analyzed the slip flow of Reiner-Rivlin fluid by a rotating disk with heat transfer. The generalized von-Kármán relations are invoked to convert the constitutive equations into similar forms. The problem is solved numerically by shooting method based on fifth-order Runge-Kutta integration scheme. The main interest here is to detect the consequences of viscoelasticity and wall roughness on the rotating disk induced flow problem. This work has been published in **Int. J. Heat & Mass Transf. 123 (2018) 979-987.**

Swirling flow of visco-plastic fluid bounded by a permeable rotating disk is also addressed in this thesis. Problem formulation is made through constitutive relations of Bingham fluid model. Entropy production analysis is made which is yet to be explored for the von-Kármán flow of non-Newtonian fluids.

Chapter 1

Introduction

This chapter contains a few important concepts related to fluid flow and heat transfer. A thorough literature survey for problems addressed in subsequent chapters is presented. Detailed explanation of the employed numerical approaches is also included.

1.1 Fundamental concepts and definitions

1.1.1 Newtonian fluids

Fluids for which shear stress is directly as well as linearly proportional to the strain rate are termed Newtonian fluids. For laminar flow between parallel plates one has:

$$\tau_{yx} = \mu \frac{du}{dy}, \tag{1.1}$$

where μ represents the coefficient of dynamic viscosity, τ_{yx} denotes the shear stress and du/dy represents the strain rate. The most common Newtonian fluids are water and air etc.

1.1.2 Non-Newtonian fluids

Non-Newtonian flows are prevalent in diverse chemical and allied processing engineering applications. Many industrial fluids including foams, slurries, emulsions and polymer melts etc.

exhibit non-Newtonian behavior meaning that their flow curve (stress vs shear rate) is non-linear and does not contain origin in general.

Non-Newtonian fluids are classified as time-independent, time-dependent and viscoelastic fluids. Time-independent fluids include pseudo-plastic fluids, dilatant fluids and visco-plastic fluids. In pseudoplastic fluids, the apparent viscosity is a decreasing function of shear rate. Whereas, the fluids for which apparent viscosity grows upon increasing shear rate are dilatant fluids. Viscoplastic materials have their ability to deform only if the shear stress reaches a minimum value called yield stress. Time dependent fluids include the thixotropic and rheopectic fluids. Viscoelastic fluids include the both viscous and elastic properties, depending upon the time scale over which an external stress is applied. A graphical representation of the non-Newtonian behavior can be clearly observed from Fig. 1.1.

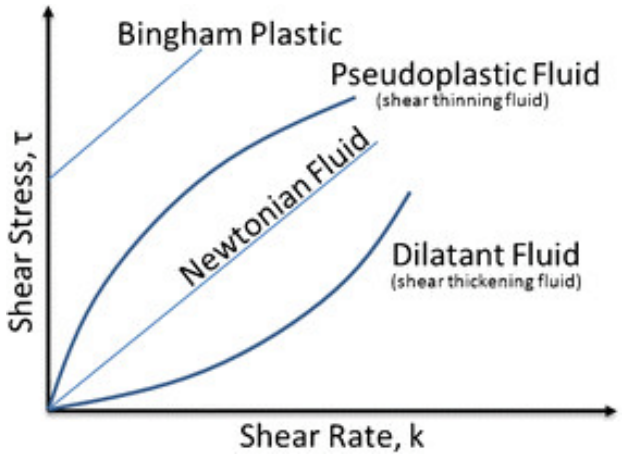

Fig. 1.1: Stress vs strain rate in non-Newtonian fluids

Two kinds of non-Newtonian fluids namely (i) viscoelastic fluids and (ii) viscoplastic fluids have been considered in this thesis.

a) Reiner-Revlin fluid model

It is viscoelastic model proposed by Reiner [23] and Revlin [24]. For this model, the shear stress τ_{ij} is expressed as follows:

$$\tau_{ij} = -p\delta_{ij} + \mu e_{ij} + \mu_c e_{ik} e_{kj} \; ; \; e_{jj} = 0, \qquad i,j = 1,2,3 \tag{1.2}$$

here p represents pressure, μ the co-efficient of dynamic viscosity, μ_c represents the cross-viscosity coefficient, δ_{ij}_shows the Kronecker delta symbol and $e_{ij} = (\partial u_i/\partial x_j + \partial u_j/\partial x_i)$ is the strain rate tensor.

b) Bingham fluid model

It is viscoplastic model, named after Professor Bingham. Its constitutive equation is given as;

$$\tau_{ij} = \begin{cases} \left(\frac{\tau_y}{\dot{\gamma}} + \mu_p\right) e_{ij} = \eta(\dot{\gamma}) e_{ij} & \text{for } \tau \geq \tau_y \,, \\ 0 & \text{for } \tau < \tau_y \,, \end{cases} \tag{1.3}$$

where $\dot{\gamma} = (1/2\; e_{ij} e_{ji})^{1/2}$ is the second invariant of the strain tensor in which $e_{ij} = (\partial u_i/\partial x_j + \partial u_j/\partial x_i)$ are components of the strain rate tensor, τ_y denotes the yield stress, μ_p defines the plastic viscosity and $\eta(\dot{\gamma})$ shows the apparent viscosity.

1.1.3 Steady and unsteady flows

In steady flow, all the fluid properties (velocity, temperature, pressure etc) at any point in the flow field are independent of time. Mathematically,

$$\frac{\partial \phi}{\partial t} = 0, \tag{1.4}$$

where ϕ is any fluid property. In case of unsteady flow, all the fluid properties at any point in the flow field are time dependent. Mathematically,

$$\frac{\partial \phi}{\partial t} \neq 0. \tag{1.5}$$

1.1.4 Incompressible and compressible flows

Flows in which density remains constant throughout the flow field are termed as incompressible flows. For incompressible flows, the Mach number is less than 0.3. However, if the fluid density

is a function of spatial coordinates then the flow is referred as compressible flow. For such flow, Mach number is greater than 0.3.

1.1.5 Laminar and turbulent flows

Laminar flow is the state of flow in which there is a smooth motion of fluid particles in parallel layers. The laminar flow occurs with the high liquid's viscosity and low Reynolds number.

The type of flow in which there is a random fluctuation and rapid mixing of fluid particles and not in parallel layers is called turbulent flow. This type of flow usually occurs with low liquid's viscosity and high Reynolds number.

1.1.6 Reynold's number

The ratio of inertial forces to the viscous forces defines the Reynold's number. Mathematically,

$$Re = \frac{\text{Inertial forces}}{\text{Viscous forces}} = \frac{\rho v L}{\mu} = \frac{vL}{\nu}, \tag{1.6}$$

where $\nu = \mu/\rho$ shows the kinematic viscosity, μ represents the dynamic viscosity, v is the average velocity and L denotes the characteristic length.

1.1.7 Prandtl number

Prandtl number is basically the ratio of kinematic viscosity to the thermal diffusivity. Mathematically,

$$Pr = \frac{\text{Kinematic viscosity}}{\text{Thermal diffusivity}} = \frac{\nu}{\alpha} = \frac{\mu/\rho}{k/\rho c_p} = \frac{\mu c_p}{k}, \tag{1.7}$$

where c_p represents the specific heat capacity and k denotes the thermal conductivity.

1.1.8 Eckert number

A dimensionless number which shows the relationship between kinetic energy and enthalpy is the Eckert number. Mathematically,

$$Ec = \frac{\text{Kinetic energy}}{\text{Enthalpy}} = \frac{v^2}{c_p \Delta T}, \tag{1.8}$$

where v denotes the average velocity of the fluid and ΔT shows the temperature difference.

1.1.9 Boundary layer

A boundary layer is the fluid layer in contact with the boundary where viscous forces alter the flow field. Fig. 1.2 shows boundary layer formulation above a flat plate at zero incidence. The fluid velocity varies from zero to the free stream velocity at the surface and boundary respectively.

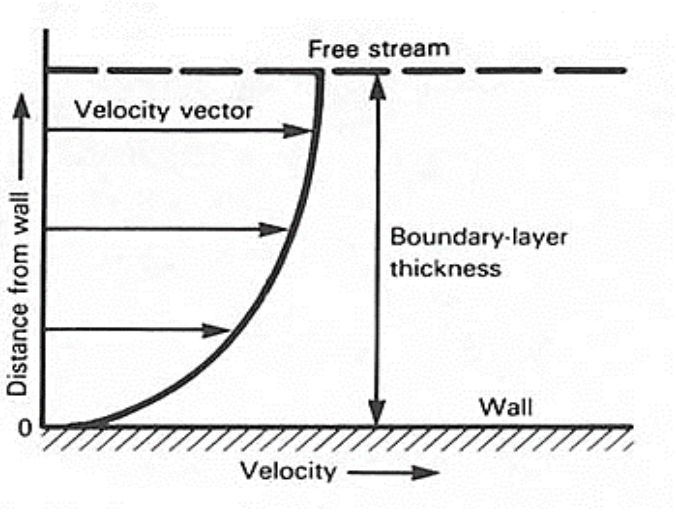

Fig. 1.2: Boundary Layer flow

1.2 von –Kármán flow -formulation and results

von-Kármán [1] considered fluid flow resulting above a disk of large radius rotating with

constant angular velocity in a calm fluid. Near the disk, due to the lack of centrifugal effect, fluid is swept away in the radial direction. Fluid above the disk replaces this fluid through a downward spiraling motion referred as "disk free pumping effect". In cylindrical coordinate system, the continuity and Navier-strokes equations describing such fluid motion are,

$$(ru)_r + (rw)_z = 0, \tag{1.9}$$

$$uu_r + wu_z - \frac{v^2}{r} = -\frac{1}{\rho}p_r + \nu\left\{u_{rr} + \frac{1}{r}u_r + u_{zz} - \frac{u}{r^2}\right\}, \tag{1.10}$$

$$uv_r + wv_z + \frac{uv}{r} = \nu\left\{v_{rr} + \frac{1}{r}v_r + v_{zz} - \frac{v}{r^2}\right\}, \tag{1.11}$$

$$uw_r + ww_z = -\frac{1}{\rho}p_z + \nu\left\{w_{rr} + \frac{1}{r}w_r + w_{zz}\right\}, \tag{1.12}$$

where u, v and w are the velocity components in the direction of increasing (r, φ, z) respectively. The boundary conditions are:

$$u = 0, v = r\omega, w = 0 \quad \text{at } z = 0, \tag{1.13}$$
$$u \to 0, v \to 0 \quad \text{as } z \to \infty.$$

Let's make use of von-Kármán transformations:

$$\eta = \sqrt{\frac{\omega}{\nu}}z \tag{1.14}$$
$$u = r\omega F(\eta), v = r\omega G(\eta), w = \sqrt{\nu\omega}H(\eta).$$

Eqs. (1.9)- (1.13) thus converted to the following ordinary differential equations.

$$H' = -2F, \tag{1.15}$$

$$F'' = F^2 - G^2 + HF', \tag{1.16}$$

$$G'' = 2FG + HG', \tag{1.17}$$

$$F = 0, G = 1, H = 0 \text{ at } \eta = 0, \tag{1.18}$$
$$F \to 0, G \to 0 \text{ as } \eta \to \infty.$$

Velocity profiles can be computed by solving Eqs. (1.15)- (1.17). Plots of the functions F, G and H are given in Fig. 1.3.

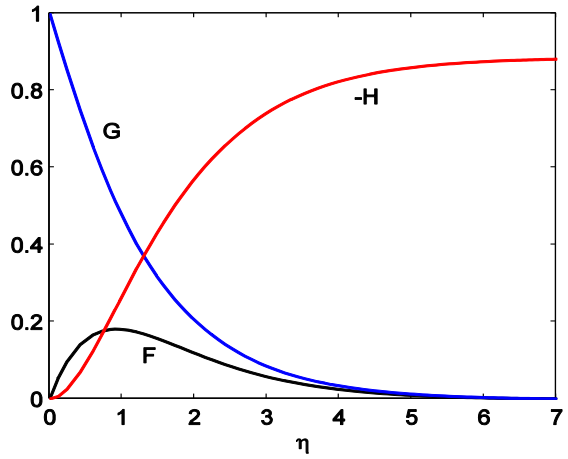

Fig. 1.3: Velocity profiles in the von-Kármán flow

1.3 Energy equation in cylindrical coordinates

Heat transfer takes place due to the temperature difference at the disk surface and that of the ambient fluid. In presence of viscous dissipation, the energy equation can be expressed in the form:

$$\rho c_p \left(u \frac{\partial T}{\partial r} + w \frac{\partial T}{\partial z} \right) = k \nabla^2 T + \Phi, \tag{1.19}$$

where k stands for thermal conductivity, c_p for the specific heat capacity and Φ represents the viscous dissipation term given below:

$$\Phi = \tau_{rr} \left(\frac{\partial u}{\partial r} \right) + \tau_{\theta\theta} \left(\frac{u}{r} \right) + \tau_{zz} \left(\frac{\partial w}{\partial z} \right) + \tau_{r\theta} \left[r \frac{\partial}{\partial r} \left(\frac{v}{r} \right) \right] + \tau_{rz} \left(\frac{\partial u}{\partial z} + \frac{\partial w}{\partial r} \right) + \tau_{\theta z} \left(\frac{\partial v}{\partial z} \right). \tag{1.20}$$

1.4 Literature review

Fluid flow induced by a rotating disk has been a compelling research topic since it is relevant in a number of technical applications involving electrochemical systems, deposition of coatings on surfaces, rotor-stator system, atmospheric and oceanic circulations, viscometer and various

others. The seminal contribution in this area was made by von-Kármán [1]. He assumed that a large disk rotates with constant angular velocity in a still fluid. Near the disk, the lack of pressure gradient to overcome centrifugal effect drives the fluid radially outward. Fluid above the disk replaces this fluid through a downward spiraling motion often referred as disk free pumping effect. von-Kármán's work has led to many subsequent research activities concerning rotating disk flows. For example, an accurate asymptotic solution to the von- Kármán's problem was presented by Cochran [2]. Heat transfer analysis for von-Kármán problem was made by Pohlhausen [3] for different values of Prandtl numbers. Suction phenomenon for fluid flow due to permeable rotating disk was investigated by Ackroyd [4]. Bachelor [5] explained that von-Kármán's problem is actually a special case of the flows resulting when disk and ambient fluid moves with separate angular velocities about the same axis. Another special case in which fluid present at infinity is in rotation while the disk is stationary was first addressed by Bödewadt [6]. A comprehensive review of literature concerning rotating disk induced flows was presented by Zandbergen and Dijkstra [7]. Miclavcic and Wang [8] modeled slip flow through a rough rotating disk and provided accurate numerical computations for broad range of slip coefficients. von- Kármán's problem was extended by Chawla et al. [9] for the case in which fluid at infinity also rotates with a different angular velocity. Turkyilmazoglu [10] explored stagnation-point flow due to stretchable rotating disk in the existence of transverse magnetic field. Recent work in this area can be seen by [11-15] and refs. there in.

Despite the fact that almost all industrial fluids are non-Newtonian, von- Kármán's analysis for non-Newtonian fluids has been scarcely attempted. Andersson et al. [16] modeled the power-law fluid flow caused by a rotating disk. They proposed a reliable numerical approach that yielded accurate numerical calculations even for highly shear-thickening fluids. Attia [17] addressed ion-slip effects on swirling flow of Reiner-Rivlin fluid caused by a rotating disk. Griffiths [18] considered the rotating flow of generalized Newtonian fluid obeying Carreau viscosity model which is practically applicable for vanishing small and very large shear rates. A mathematical model for flow of power-law fluid induced by a rotating disk having variable thickness was developed by Xun et al. [19]. Very recently, Muthtamilselvan [20] described thermophoretic diffusion in steady micropolar fluid flow due to rotating disk. However modest attention is paid towards the treatment of von-Kármán flow problem involving non-Newtonian fluids.Heat

transfer to von Kármán flow of power-law fluid was considered by Ming et al. [21] through a generalized Fourier model based on temperature dependent thermal conductivity.

Fluids such as large molecular weight polymers that do not follow the Newtonian constitutive relation are frequently encountered in chemical and plastic industries. Paints, clay, nylon, slurries, detergents, blood, lubricants, colloids, melted chocolate, egg whites, mayonnaise, gelatin etc. exhibit non-Newtonian behavior. The stress inside viscoelastic fluids does not vanish instantly upon the removal of stress due to sustained stress by intermolecular structure. This unique characteristic is termed as memory effect. The non-Newtonian fluid model given by Reiner [22] and Rivlin [23] can adequately predict flow behaviors of many geological and biological materials as well as many food products and polymers. A few recent examples can be found through [24-30].

Among various classes of non-Newtonian materials are those exhibiting viscoplastic properties due to their ability to deform only if the shear stress reaches a certain minimum value called yield stress. Waxy crude oils, paints, jellies, emulsions, pastes and foams are common viscoplastic materials. Bingham fluid model is perhaps the simplest possible representation of the viscoplastic behavior. On the other hand, heat transfer phenomenon is associated with fluid flows in wide spectrum of engineering and geophysical applications. Heat transfer plays enormous role in many industrial sectors such as in energy production, in automotive industry, in chemical and food processing industries, in home appliances and in aerospace engineering. Ahmadpour and Sadeghy [31] explored the von-Kármán problem for Bingham fluids. Their analysis revealed that yield stress in Bingham fluid contributes to a growth in minimum torque needed to maintain steady disk rotation. Similar problem was re-investigated in a later paper by Guha and Sengupta [34] with a focus on different computational approaches. Very recently, Tabassum and Mustafa [35] examined the von-Kármán flow of Reiner-Rivlin fluid subject to partial slip using shooting method.

1.5 Numerical methods

1.5.1 Shooting method

Shooting method is a numerical technique which is utilized to solve the non-linear boundary value problem. At first, the boundary value problem (BVP) is changed into the initial value problem (IVP).

Let us consider the second order ordinary differential equation;

$$p'' = f(x, p, p'), \qquad a \leq x \leq b \tag{1.21}$$

subject to the boundary conditions:

$$p(a) = C_1, \;\; p(b) = C_2 \tag{1.22}$$

where a, b, C_1 and C_2 are constants.

To reduce the second order ODE into first order, we substitute;

$$x_1 = p, \;\; x_1' = x_2 = p' \tag{1.23}$$

Thus the Eq. (1.22) and (1.23) takes the form;

$$x_1(a) = C_1, \quad x_1'(a) = \lambda(\text{unknown}) \tag{1.24}$$

Here λ is the unknown parameter whose value has to be determined.

$$\lim_{k\to\infty} p(b, \lambda_k) = p(b) = C_2 \tag{1.25}$$

A sequence of $\lambda_1, \lambda_2, \lambda_3, \ldots$ is produced through λ_o as an initial guess. The iteration must stop when;

$$p(b, \lambda) - C_2 = 0 = \Phi(\lambda) \tag{1.26}$$

We get the solution for (1.23) and (1.24) through RK-5 by taking λ_o as initial value. After implementing RK-5, we take into account the Newton's method. Newton's Raphson formula is employed to generate the sequence. It is defined as;

$$\lambda_{n+1} = \lambda_n - \frac{\Phi(\lambda_n)}{\frac{d\Phi(\lambda_n)}{d\lambda}} \tag{1.27}$$

1.5.2 bvp4c

A programming in MATLAB requires a guess to solve the boundary value problem (BVP). bvp4c solver of commercial software MATLAB is very effective to solve the BVP. As shooting technique is not as vigorous as collocation or finite difference method, we have used bvp4c. This technique is based on the collocation method which gives solution on the mesh x_i $(i = 1,2,\cdots N)$. For the sake of accuracy a different step size can also be used. In contrast to shooting method the solution in bvp4c is estimated over the entire interval and the boundary conditions are also taken into account all the time. [39].

Chapter 2

Numerical solutions for von-Kármán flow of Reiner-Rivlin fluid with slip conditions

2.1 Introduction

This chapter deals with the partial slip flow of Reiner-Rivlin fluid induced by a rough rotating disk. Heat transfer is also inspected by assuming more general temperature jump condition. The constitutive relations in Reiner-Rivlin fluid lead to a coupled and strongly non-linear differential system. A convenient numerical treatment is invoked to solve the resulting similarity equations for broad ranges of non-Newtonian fluid parameter and slip coefficients. Our main interest is to predict the behaviors of fluid elasticity and wall slip coefficients on the von-Kármán flow problem. Expressions of wall skin friction and surface heat transfer are calculated and deliberated for broad parameter values. Different from radial and axial velocities, tangential velocity appears to increase as Reiner-Rivlin fluid parameter (K) increases. Reduction in surface drag coefficient, which is vital in some applications, can be accomplished by increasing the parameter K. Volumetric flow rate is also inversely proportional to the parameter K. However, heat transfer rate diminishes when parameter K enlarges. We also conclude that larger torque would be required to keep steady rotation of the disk for higher values of wall slip coefficients.

2.2 Problem formulation

Consider an incompressible Reiner-Rivlin fluid occupying semi-infinite region above a disk

(with large radius R) residing in the plane $z = 0$. The disk is in a state of rigid body rotation about the axis $r = 0$ with uniform angular velocity ω that sets up a swirling flow in the neighboring fluid layers. Let (u, v, w) be the velocities along (r, φ, z) directions respectively. Because of the axial symmetry, the velocity components are assumed to be φ-independent. Partial slip conditions are treated. According to Reiner [23] and Rivlin [24], the stress tensor has the following form:

$$\tau_{ij} = -p\delta_{ij} + \mu e_{ij} + \mu_c e_{ik} e_{kj} \; ; \; e_{jj} = 0, \tag{2.1}$$

in which p represents pressure, μ is the co-efficient of dynamic viscosity, μ_c represents the cross-viscosity coefficient, δ_{ij} is the Kronecker symbol and $e_{ij} = (\partial u_i/\partial x_j + \partial u_j/\partial x_i)$ denotes the strain rate tensor. Relevant equations describing fluid motion and heat transfer over a rotating disk are given below:

$$\frac{\partial u}{\partial r} + \frac{u}{r} + \frac{\partial w}{\partial z} = 0, \tag{2.2}$$

$$\rho\left(u\frac{\partial u}{\partial r} + w\frac{\partial u}{\partial z} - \frac{v^2}{r}\right) = \frac{\partial \tau_{rr}}{\partial r} + \frac{\partial \tau_{rz}}{\partial z} + \frac{\tau_{rr} - \tau_{\varphi\varphi}}{r}, \tag{2.3}$$

$$\rho\left(u\frac{\partial v}{\partial r} + w\frac{\partial v}{\partial z} + \frac{uv}{r}\right) = \frac{1}{r^2}\frac{\partial}{\partial r}\left(r^2\tau_{r\varphi}\right) + \frac{\partial \tau_{z\varphi}}{\partial z} + \frac{\tau_{r\phi} - \tau_{\phi r}}{r}, \tag{2.4}$$

$$\rho\left(u\frac{\partial w}{\partial r} + w\frac{\partial w}{\partial z}\right) = \frac{1}{r}\frac{\partial(r\tau_{rz})}{\partial r} + \frac{\partial \tau_{zz}}{\partial z}, \tag{2.5}$$

$$\rho c_p\left(u\frac{\partial T}{\partial r} + w\frac{\partial T}{\partial z}\right) = k\frac{\partial^2 T}{\partial z^2}, \tag{2.6}$$

where ρ stands for fluid density, k for thermal conductivity and c_p for the specific heat capacity. The last term in Eq. (2.4) can be omitted by employing symmetry for the stress tensor components. For the present flow i.e. axi-symmetric, the strain rate components are given below [31]:

$$\begin{gathered} e_{rr} = 2\frac{\partial u}{\partial r}, e_{\theta\theta} = 2\frac{u}{r}, e_{zz} = 2\frac{\partial w}{\partial z}, e_{r\theta} = e_{\theta r} = r\frac{\partial}{\partial r}\left(\frac{v}{r}\right), \\ e_{z\theta} = e_{\theta z} = \frac{\partial v}{\partial z}, e_{rz} = e_{zr} = \frac{\partial u}{\partial z} + \frac{\partial w}{\partial r}. \end{gathered} \tag{2.7}$$

Through definition (2.1), the stress tensor components are obtained as follows:

$$\tau_{rr} = -p + \mu\left(2\frac{\partial u}{\partial r}\right) + \mu_c\left\{4\left(\frac{\partial u}{\partial r}\right)^2 + \left(\frac{\partial v}{\partial r} - \frac{v}{r}\right)^2 + \left(\frac{\partial u}{\partial z} + \frac{\partial w}{\partial r}\right)^2\right\}, \tag{2.8}$$

$$\tau_{zr} = \mu\left(\frac{\partial u}{\partial z} + \frac{\partial w}{\partial r}\right) + \mu_c\left\{\left(2\frac{\partial u}{\partial r}\right)\left(\frac{\partial u}{\partial z} + \frac{\partial w}{\partial r}\right) + \left(\frac{\partial v}{\partial r} - \frac{v}{r}\right)\left(\frac{\partial v}{\partial z}\right) + \left(\frac{\partial u}{\partial z} + \frac{\partial w}{\partial r}\right)\left(2\frac{\partial w}{\partial z}\right)\right\}, \tag{2.9}$$

$$\tau_{\varphi\varphi} = -p + \mu\left(\frac{2u}{r}\right) + \mu_c\left\{\frac{4u^2}{r^2} + \left(\frac{\partial v}{\partial r} - \frac{v}{r}\right)^2 + \left(\frac{\partial v}{\partial z}\right)^2\right\}, \tag{2.10}$$

$$\tau_{r\varphi} = \mu\left(\frac{\partial v}{\partial r} - \frac{v}{r}\right) + \mu_c\left\{\left(2\frac{\partial u}{\partial r}\right)\left(\frac{\partial v}{\partial r} - \frac{v}{r}\right) + \left(\frac{\partial v}{\partial r} - \frac{v}{r}\right)\left(\frac{2u}{r}\right) + \left(\frac{\partial u}{\partial z} + \frac{\partial w}{\partial r}\right)\left(\frac{\partial v}{\partial z}\right)\right\}, \tag{2.11}$$

$$\tau_{z\varphi} = \mu\frac{\partial v}{\partial z} + \mu_c\left\{\left(\frac{\partial v}{\partial r} - \frac{v}{r}\right)\left(\frac{\partial u}{\partial z} + \frac{\partial w}{\partial r}\right) + 2\left(\frac{u}{r}\right)\left(\frac{\partial v}{\partial z}\right) + 2\left(\frac{\partial v}{\partial z}\right)\left(\frac{\partial w}{\partial z}\right)\right\}, \tag{2.12}$$

$$\tau_{zz} = -p + \mu\left(2\frac{\partial w}{\partial z}\right) + \mu_c\left\{\left(\frac{\partial u}{\partial z} + \frac{\partial w}{\partial r}\right)^2 + \left(\frac{\partial v}{\partial z}\right)^2 + 4\left(\frac{\partial w}{\partial z}\right)^2\right\}. \tag{2.13}$$

Assuming no penetration at the disk, partial slip conditions for present flow can be expressed as follows:

$$u(r,0) = \beta_1\tau_{rz}(r,0)\ , v(r,0) = \beta_2\tau_{z\varphi}(r,0) + r\omega\ , w = 0\ , \quad T(r,0) = T_w + \beta_3 T_z(r,0). \tag{2.14a}$$

in which β_1 denotes the radial slip coefficient, β_2 is the azimuthal slip coefficient and γ represents the thermal slip coefficient. Since lateral velocities and temperature difference are zero far from the disk so we have

$$u(r,z) \to 0\ , v(r,z) \to 0, T(r,z) \to T_\infty \text{as } z \to \infty. \tag{2.14b}$$

Let us introduce the following self-similar transformations in terms of dimensionless distance $\zeta = (\omega/\nu)^{1/2}z$:

$$(u,v,w) = \left(r\omega F'(\zeta), r\omega G(\zeta), -2\sqrt{\nu\omega}\,F(\zeta)\right), \quad (p,T) = \left(p_\infty - \omega\mu P(\zeta), T_\infty + (T_w - T_\infty)\theta(\zeta)\right), \tag{2.15}$$

where prime indicates differentiation with respect to ζ. Note that Eq. (2.1) is identically satisfied by transformations (2.15) and Eqs. (2.2)-(2.4) convert into the following ordinary differential equations:

$$F''' - F'^2 + 2FF'' + G^2 + K(F''^2 - 2F'F''' - G'^2) = 0, \tag{2.16}$$

$$G'' - 2F'G + 2FG' + 2K(F''G' - F'G'') = 0, \tag{2.17}$$

$$\theta'' + 2PrF\theta' = 0. \tag{2.18}$$

In the above equations, $Pr = \mu c_p/k$ denotes the Prandtl number and $K = \mu_C\,\omega/\mu$ is material parameter of Reiner-Rivlin fluid. Let us define:

$$\lambda_1 = \rho(\omega\nu)^{1/2}\beta_1, \lambda_2 = \rho(\omega\nu)^{1/2}\beta_2, \gamma = (\omega/\nu)^{1/2}\beta_3. \tag{2.19}$$

Using (2.15), the boundary conditions (2.14a) and (2.14b) are converted into the following forms:

$$F'(0) = \lambda_1[F''(0) - 2KF'(0)F''(0)]\,, G(0) = \lambda_2[G'(0) - 2KG'(0)F'(0)] + 1, \tag{2.20a}$$

$$\theta(0) = 1 + \gamma\theta'(0),$$

$$F' \to 0,\;\; G \to 0\,, \theta \to 0 \quad as \;\; \zeta \to \infty. \tag{2.20b}$$

The presence of viscosity near the disk produces tangential stress at the disk which resists its rotation. Torque T_0 needed to maintain steady rotation of disk with radius R is measured through the definite integral:

$$T_0 = -\int_0^R \tau_{z\varphi}\big|_{z=0}(2\pi r^2)dr = -\frac{\pi\rho\omega}{2}\sqrt{\nu\omega}R^4G'(0)\,. \tag{2.21}$$

Quantity of prime interest in this work is the skin friction coefficient C_f defined as under:

$$C_f = \frac{\sqrt{\tau_r^2 + \tau_\varphi^2}}{\rho(r\Omega)^2}, \tag{2.22}$$

where τ_r and τ_ϕ denote the radial and azimuthal wall stresses. Through variables (2.15), Eq. (2.22) assumes the following form:

$$C_f = \left(\frac{\omega r^2}{\nu}\right)^{-1/2}\sqrt{(F''(0))^2 + \big(G'(0)\big)^2}. \tag{2.23}$$

Local Nusselt number Nu can be obtained from the Fourier law as follows:

$$Nu = \frac{Lq_w}{k(T_w - T_\infty)} = -\theta'(0). \tag{2.24}$$

where q_w denotes the wall heat flux and $L = \sqrt{\nu/\omega}$ is the length scale.

Additionally, the total amount of fluid drawn in the axial direction can be measured through $F(\infty)$. Thus numerical computations for $F''(0), G'(0), \theta'(0)$ and $H(\infty)$ will be made to understand physical aspects of the problem.

2.3 Numerical approach

The governing equations posed by (2.16)-(2.18) together with the conditions (2.20a) and (2.20b) is a boundary value problem having no exact solution near to sight. Thus we take into account the conventional shooting approach to seek a numerical solution of the problem. Let us convert Eqs. (2.16)-(2.18) into a system of first-order equations by substituting $z_1 = F, z_2 = F', z_3 = F'', z_4 = G,\ z_5 = G', z_6 = \theta, z_7 = \theta'$. We obtain the following:

$$
\begin{aligned}
&z_1' = z_2; && z_1(0) = 0,\\
&z_2' = z_3; && z_2(0) = \lambda_1[z_3(0) - 2Kz_2(0)z_3(0)],\\
&z_3' = \frac{z_2^2 - 2z_1z_3 - z_4^2 - Kz_3^2 + Kz_5^2}{1 - 2Kz_2}; && z_3(0) = u(1),\\
&z_4' = z_5; && z_4(0) = \lambda_2[z_5(0) - 2Kz_5(0)z_2(0)] + 1,\\
&z_5' = \frac{2z_2z_4 - 2z_1z_5 - 2Kz_3z_5}{1 - 2Kz_2}; && z_5(0) = u(2),\\
&z_6' = z_7; && z_6(0) = 1 + \gamma z_7(0),\\
&z_7' = -2Prz_1z_7; && z_7(0) = u(3).
\end{aligned}
\tag{2.25}
$$

To solve the above system numerically, we implement Runge-Kutta method of fifth order considering suitable guesses for the unknown slopes $u(1), u(2)$ and $u(3)$. The exact values of these slopes are iteratively computed through Newton's method. In the course of computations, the step size $h = 0.01$ is chosen while residual of boundary conditions at infinity is assumed to be 10^{-5}.

2.4 Results and discussion

Slip flow of Reiner-Rivlin fluid caused by an infinite rotating disk is modeled here. Additionally, general temperature jump conditions are treated for analyzing the thermal field. Numerical

calculations are successfully carried out for wide ranges of wall roughness parameters λ_1 and $\lambda_2$and Reiner-Rivlin fluid parameter K. Validation of the numerical scheme is made by comparing the computational results of $F''(0), G'(0)$ and $F(\infty)$ with available study [11] in the Newtonian fluid case. Table 2.1 demonstrates that our numerical findings are virtually similar to those found by [11] for all values of wall roughness parameters.

Table 2.2 computes the radial wall stress $F''(0)$azimuthal wall stress $G'(0)$and entrainment velocity $F(\infty)$for various parameter values. As described in [31], the entrainment velocity $F(\infty)$ measures the volumetric flow rate of the von-Kármán problem. Also tangential stress at the wall measures the driving torque on the disk of radius R. The results predict that driving torque in von-Kármán's problem can be reduced by considering viscoelastic effects. However, an increment in either radial or azimuthal slip coefficient substantially elevates the resisting torque as well as the skin friction factor. This implies that one requires larger torque at the shaft of the disk if the azimuthal wall coefficient is higher.

Table 2.3 includes the local Nusselt number data obtained at different values of Reiner-Rivlin fluid parameter K and thermal slip parameter γ. It can be realized that by increasing elasticity parameter K heat transfer rate should elevate. However, the influence of thermal slip coefficient appears to be qualitatively opposite to that of parameter K. Thus we conclude that heat penetration depth shortens when thermal slip coefficient enlarges. As Prandtl number Pr enlarges, heat transfer rate grows further as anticipated.

In Figs. 2.1a-2.1d, velocity and temperature distributions are obtained for various wall roughness parameters in Newtonian fluid case ($K = 0$). In these Figures, it is assumed that radial and azimuthal slip coefficients are equal. In absence of slip, the radial velocity profile F' starts from zero at the disk and reaches a maximum value and then asymptotically vanishes outside the boundary layer. It can be noticed that, that location of maximum velocity moves near the wall as slip effect gets strengthened. Cross-over in the curves of F' is also apparent near $\zeta = 4$ depicting that radial velocity decreases near the disk and increases away from it with an increment in wall roughness parameters. Wall slip also tends to reduce the induced axial motion far from the disk but not near the wall regions. The azimuthal velocity component v is also reduced when wall roughness parameters are simultaneously increased. This is because the rotational effect of the disk is partially transferred in the neighboring fluid layers because of which azimuthal velocity

component decreases. Dissimilar to the velocity profiles, temperature profiles appear to increase for increasing values of wall roughness parameters. Figs. 2.2a-2.2d include the corresponding results in case of Reiner-Rivlin fluid with $K = 1$. It is intriguing to witness that the variation in velocity and temperature profiles with λ_1 and λ_2 appears to be of similar magnitude in Newtonian and Reiner-Rivlin fluids.

Figs. 2.3a-2.3d reveal the velocity and temperature curves for different values of Reiner-Rivlin fluid parameter K in uniform roughness case ($\lambda_1 = \lambda_2 = 1$). Radial velocity profile, represented by function F', decreases near to the disk and increases away from it when K is incremented. The location of absolute maximum also occurs at a lower vertical distance when larger K is considered. Axial flow decelerates as parameter K enlarges. Physically, less amount of fluid is drawn axially and pushed away in the radial direction as viscoelastic effects are enhanced. It can be concluded that centrifugal fan like behavior in classical von-Kármán problem is also preserved in the non-Newtonian case. Dissimilar to the radial and axial velocity distributions, the azimuthal velocity profile G grows for increasing values of Reiner-Rivlin fluid parameter K. Like azimuthal velocity component G, temperature θ is also seen to increase as parameter K is increased. The results corresponding to the no-slip case are displayed in Figs. 2.4a-2.4d. The parameter range for Reiner-Rivlin fluid parameter K is similar to that of Figs. 2.3a-2.3d. Although the effects of K on profiles are similar to those encountered in the slip case, but the effects appear to be prominent in the no-slip case.

Figs. 2.5a and 2.5b display the evolution of temperature profiles for different values of thermal slip parameter γ. In absence of temperature jump, the profile begins from unity at the disk and approaches to zero value in asymptotic fashion. It is pertinent to mention that viscous dissipation effect, which is expected in high speed flows, is ignored here. Consideration of temperature jump allows the heat to be partially transferred in the fluid layers which in turn reduces fluid temperature. Increasing Prandtl number also leads to a reduction in heat penetration depth which yields thinner temperature profiles.

Table 2.1: Comparison of present findings with those of Turkyilmazoglu and Senel [11] in uniform roughness case ($\lambda_1 = \lambda_2$)with $K = 0$.

λ_1	λ_2	$F''(0)$[a]	$G'(0)$[a]	$F(\infty)$[a]	$F''(0)$[b]	$G'(0)^b$	$F(\infty)^b$
0	0	0.5102326	-0.6159220	0.442237	0.5102332	-0.6159219	0.442228
1	1	0.1279236	-0.3949276	0.394738	0.1279241	-0.3949280	0.394713
5	5	0.0185885	-0.1433882	0.291882	0.0185883	-0.1433879	0.291842
10	10	0.0068125	-0.0810300	0.243792	0.0068125	-0.0810301	0.243797
20	20	0.0023615	-0.0437884	0.199987	0.0023615	-0.0437883	0.199904
40	40	0.0007901	-0.0229953	0.162113	0.0007899	-0.0229951	0.160963

[a] Denotes results obtained by Turkyilmazoglu and Senel [11].

[b] Denotes results obtained by present authors.

Table 2.2: Computational results of $F''(0), G'(0), F(\infty)$ and $\sqrt{(F''(0))^2 + (G'(0))^2}$ for various values of λ_1, λ_2 and K.

λ_1	λ_2	K	$F(\infty)$	$F''(0)$	$G'(0)$	$\sqrt{(F''(0))^2 + (G'(0))^2}$
0	1	1	0.311709	0.207331	-0.358186	0.413859
1	1	1	0.344454	0.115547	-0.434954	0.450038
5	1	1	0.370581	0.046260	-0.495405	0.497560
10	1	1	0.377733	0.0269286	-0.512596	0.513302
20	1	1	0.382165	0.014736	-0.523517	0.523724
40	1	1	0.384371	0.007747	-0.529797	0.529853
1	0	1	0.391597	0.164954	-0.815806	0.832315
1	1	1	0.344454	0.115547	-0.434952	0.450038
1	5	1	0.259799	0.053222	-0.149826	0.158998
1	10	1	0.217807	0.033271	-0.083031	0.089448
1	20	1	0.164482	0.019748	-0.044254	0.048460
1	40	1	0.130641	0.011342	-0.023059	0.025689
1	1	0	0.394633	0.127922	-0.394925	0.419473
1	1	2	0.292088	0.077918	-0.424422	0.431515
1	1	4	0.224873	0.033996	-0.351571	0.353210
1	1	6	0.187214	0.020212	-0.304642	0.305309
1	1	8	0.166741	0.014231	-0.272431	0.272802

Table 2.3: Results of $\theta'(0)$ for changing values of K, γ and Pr when $\lambda_1 = \lambda_2 = 1$.

K	γ	Pr	$\theta'(0)$
0	1	7	-0.533151
2	1	7	-0.453112
4	1	7	-0.370251
6	1	7	-0.322063
8	1	7	-0.289552
1	0	7	-1.003961
1	1	7	-0.500988
1	5	7	-0.166776
1	10	7	-0.090941
1	20	7	-0.047628
1	40	7	-0.024392
1	1	2	-0.343431
1	1	3	-0.394310
1	1	7	-0.500988
1	1	10	-0.544940

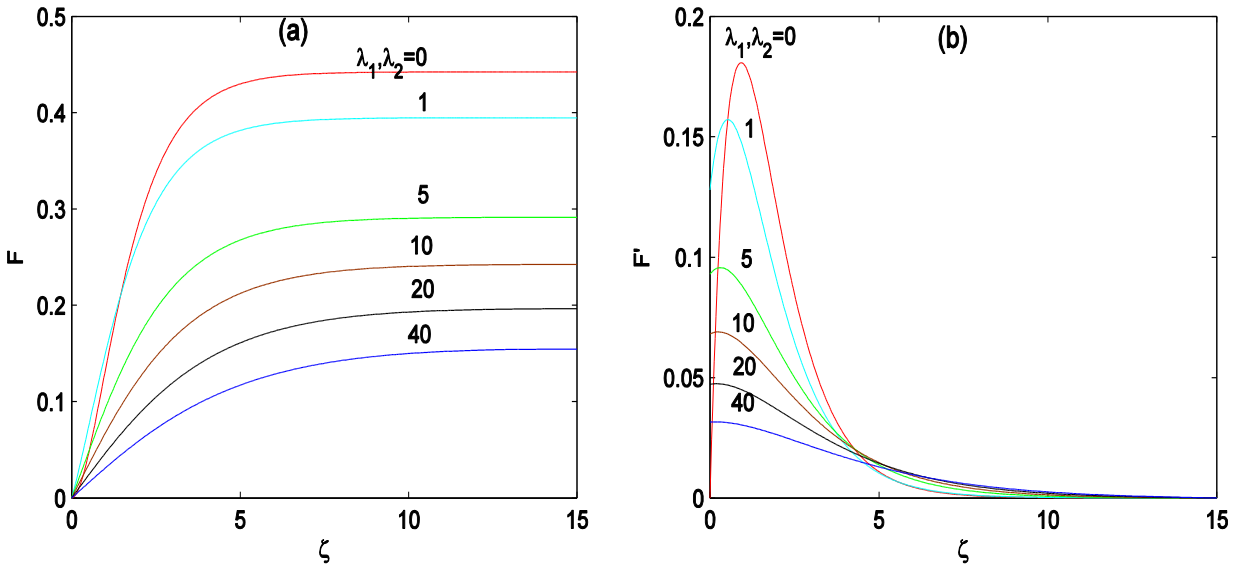

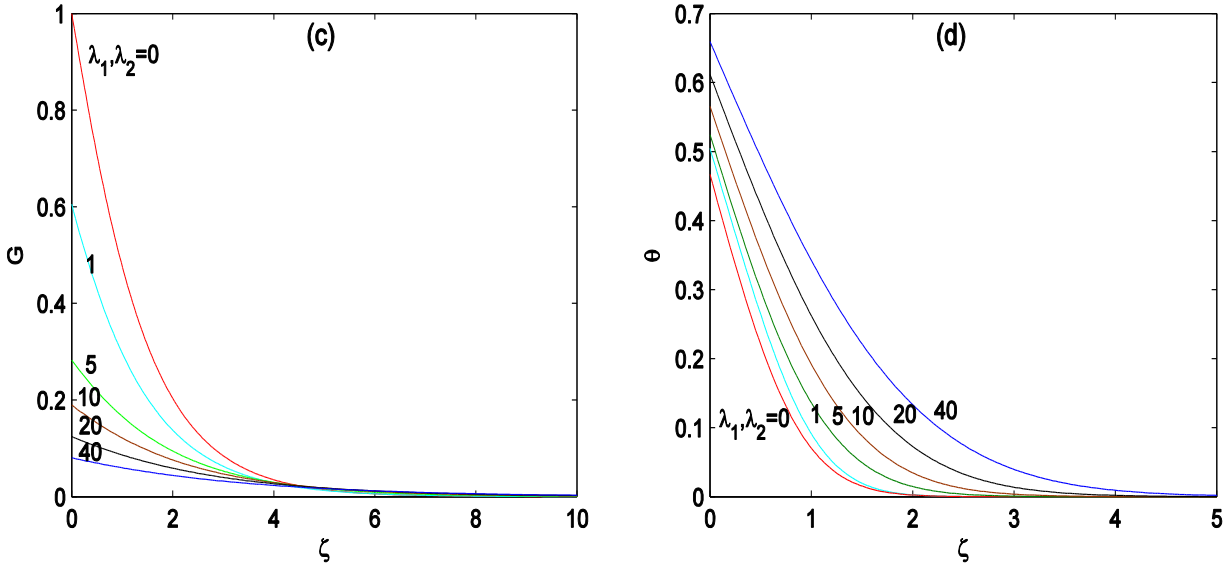

Fig. 2.1: Velocity profiles and temperature profiles for various values of wall roughness parameters λ_1 and λ_2 in Newtonian fluid case ($K = 0$) with $Pr = 7$and $\gamma = 1$.

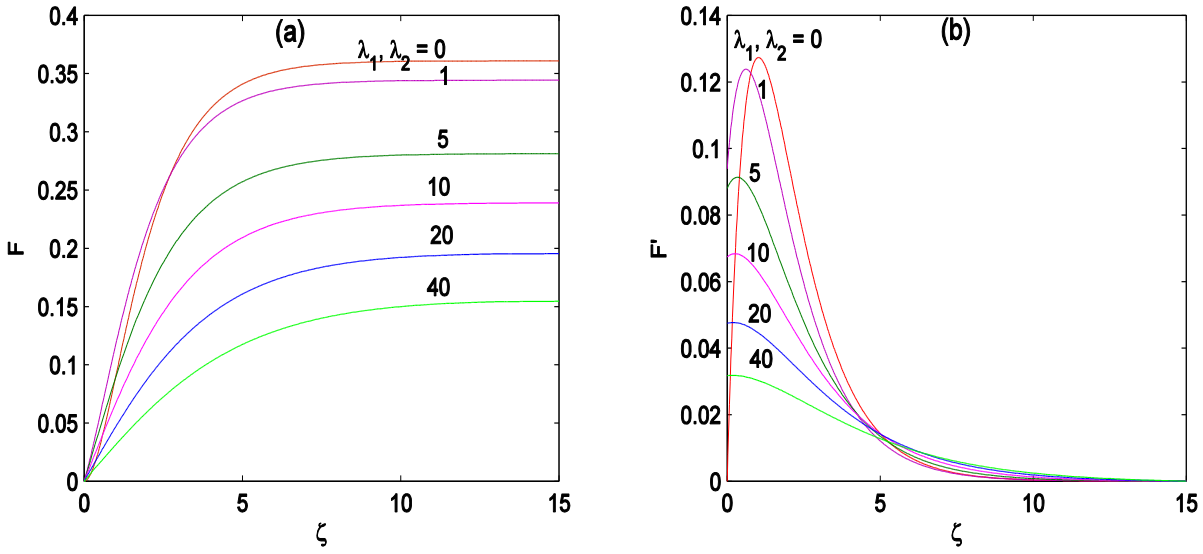

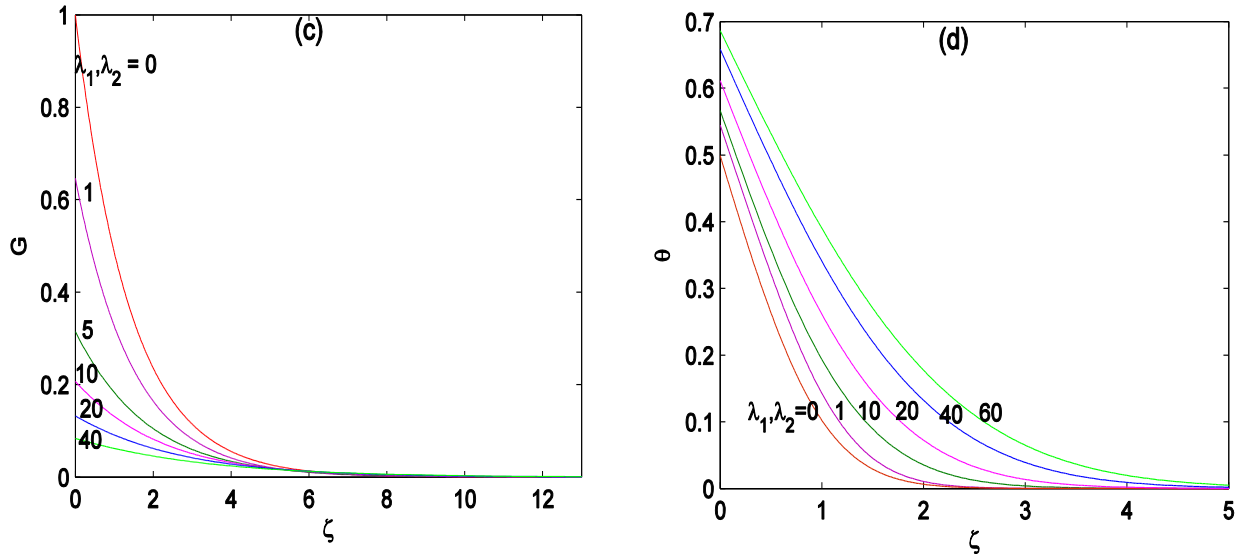

Fig. 2.2: Results of velocities and temperature for various values of wall roughness parameters λ_1 and λ_2 in non-Newtonian fluid case ($K = 1$) with $Pr = 7$and $\gamma = 1$.

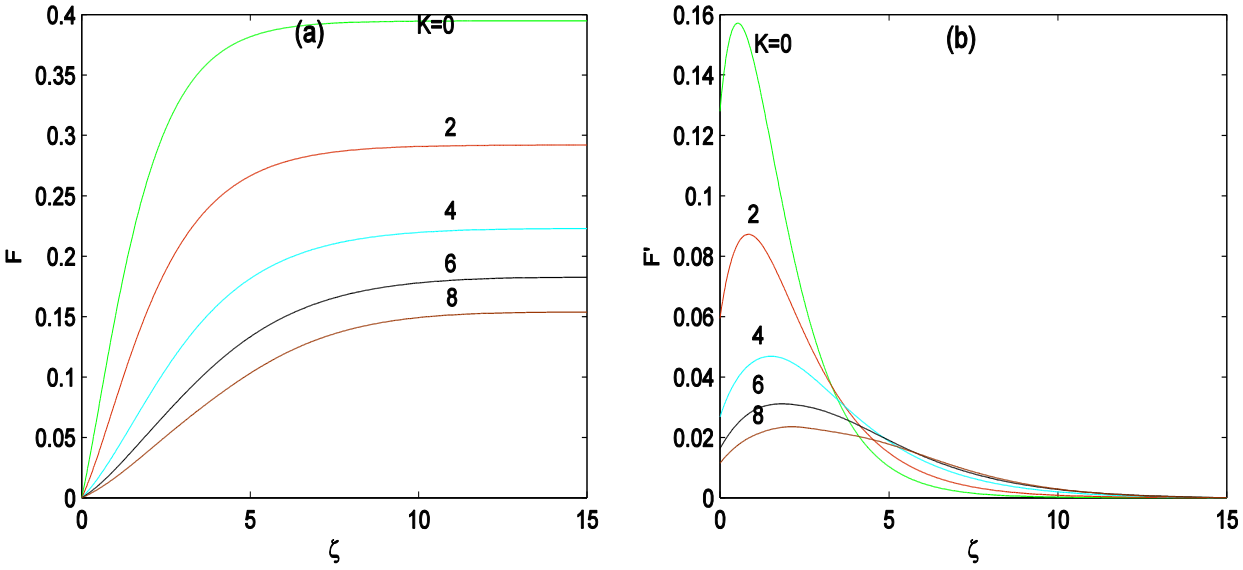

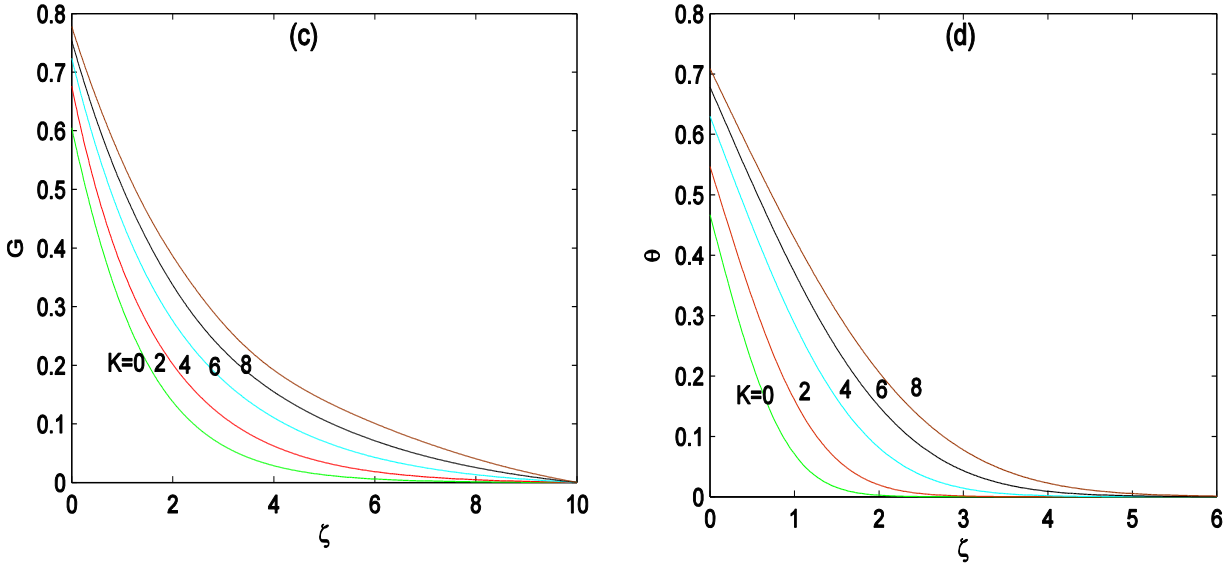

Fig. 2.3: Profiles of velocity and temperature for various values of Reiner-Rivlin fluid parameter K when $\lambda_1 = \lambda_2 = \gamma = 1$and $Pr = 7$.

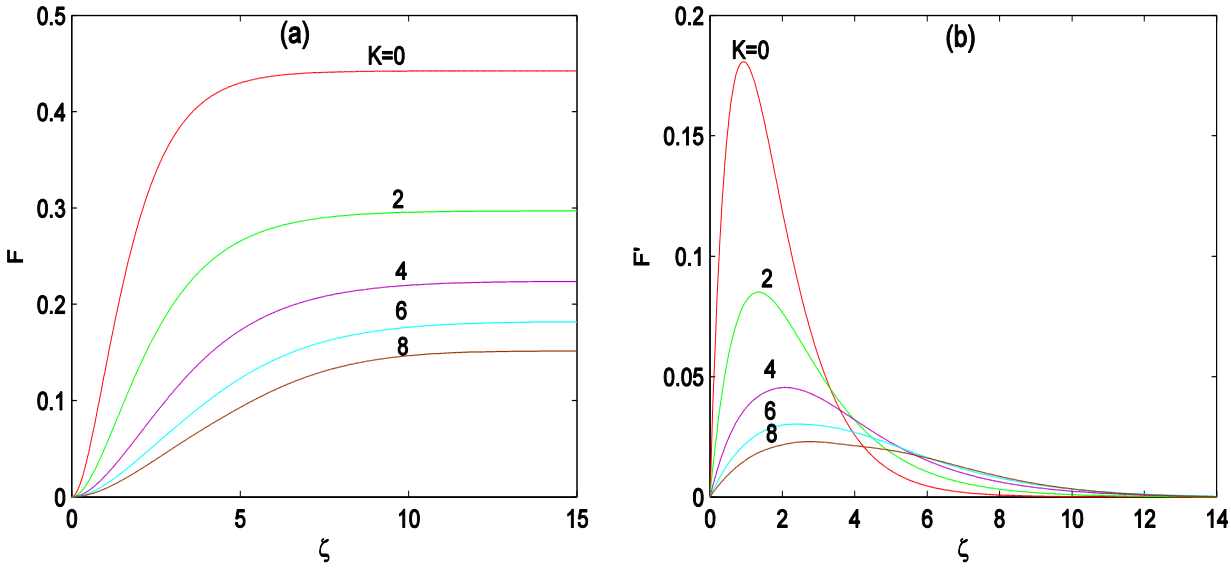

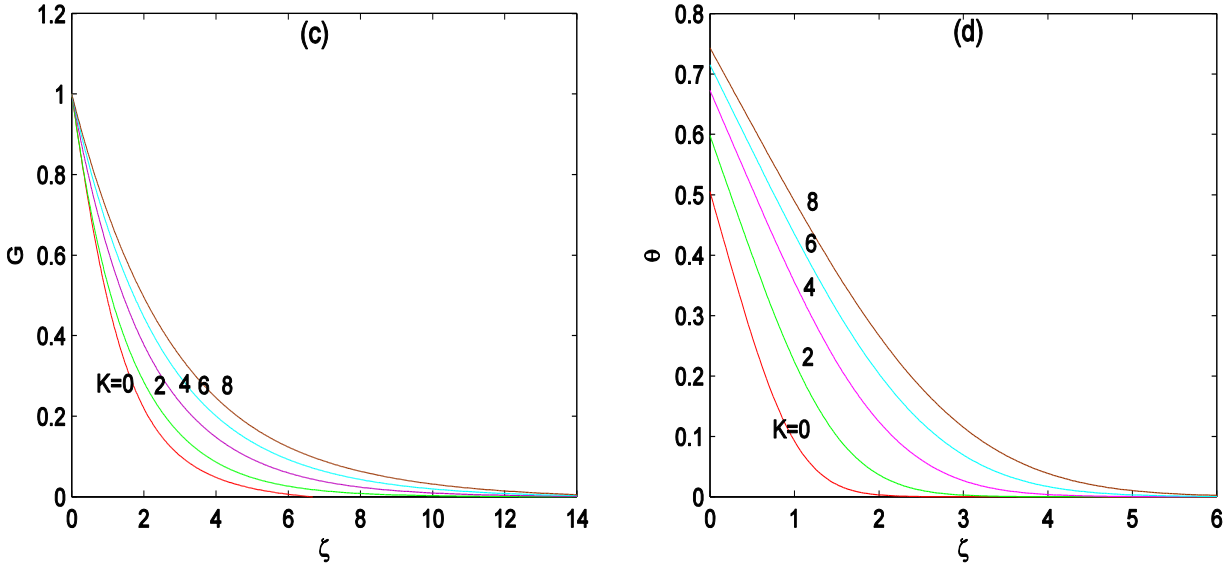

Fig. 2.4: Profiles of velocity and temperature for various values of Reiner-Rivlin fluid parameter K in no-slip case when $\gamma = 1$ and $Pr = 7$.

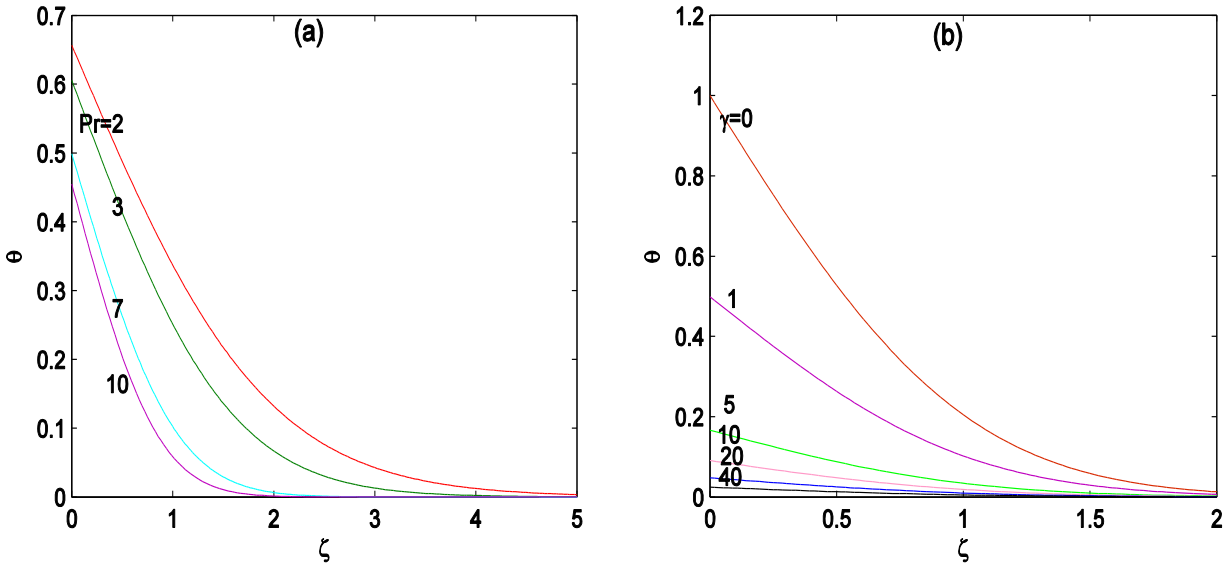

Fig. 2.5: Profiles of temperature θ for different values of (a) Prandtl number Pr and (b) thermal slip parameter γ.

2.5 Conclusions

Partial slip flow along with heat transfer of Reiner-Rivlin fluid induced by a rough rotating disk is explored. With the aid of von-Kármán self-similar transformations, similarity solutions are found for full range of slip coefficients. The numerical solution enabled us to examine the role of main physical attributes of the problem namely viscoelasticity and wall roughness effects. Following observations are made on the basis of present analysis:

1. Radially outward flow near the disk developed by disk centrifugal effect decelerates as the Reiner-Rivlin fluid parameter K is incremented.
2. Reductions in driving torque and skin friction factor are anticipated for increasing viscoelastic effects.
3. For increasing wall roughness parameters λ_1 and λ_2, increasing trends in resisting torque and skin friction factor are found. Entrainment velocity appears to reduce as the slip effect becomes stronger.
4. A decrease in the radial velocity profile near the disk and increase by moving away from it is observed as the wall roughness parameters increase.
5. Temperature profile is inversely proportional to the wall roughness parameters. Thermal boundary layer expands when Reiner-Rivlin fluid parameter K increases.
6. Thermal boundary layer shrinks and heat transfer rate enhances as the thermal slip parameter is incremented.
7. Viscoelastic effect enhances temperature profile but reduces the magnitude of local Nusselt number.

Chapter 3

Heat transfer effects on laminar flow of Bingham fluid by a rotating disk with suction: Entropy generation analysis

3.1 Introduction

In this chapter we discuss heat transfer to swirling flow of viscoplastic fluid bounded by a permeable rotating disk. Problem formulation is made through constitutive relations of Bingham fluid model. Viscous dissipation effects are also factored in the analysis. Entropy production analysis is made which is yet to be explored for the von-Kármán flow of non-Newtonian fluids. Having found the similarity equations, these have been dealt numerically for broad parameter values. The solutions are remarkably influenced by wall suction parameter (A) and Bingham number (Bn) proportional to the fluid yield stress. Akin to earlier numerical results, thermal boundary layer appears to suppress upon increasing the strength of wall suction. Thermal penetration depth is much enhanced when fluid yield stress becomes large. Higher heat transfer rate can be accomplished by employing higher suction at the disk. However, a deterioration in heat transfer is anticipated by increasing fluid yield stress. Current numerical results are in perfect line with those of an existing article in limiting sense.

3.2 Problem formulation

Suppose a permeable disk of large radius R lying in the plane $z = 0$ rotates with constant angular

velocity in an otherwise stationary viscoplastic fluid obeying Bingham fluid model. All three velocities u, v and w will be non-zero and, owing to the rotational symmetry, these will not change with respect to azimuthal coordinate θ. The disk temperature is considered as constant at T_w while T_∞ denotes the temperature outside the thermal boundary layer. Heat generation due to fluid friction will be factored in the analysis. Relevant equations describing fluid motion and heat transfer above a rotating disk can be cast into the following forms:

$$\frac{\partial u}{\partial r}+\frac{u}{r}+\frac{\partial w}{\partial z}=0, \tag{3.1}$$

$$\rho\left(u\frac{\partial u}{\partial r}+w\frac{\partial u}{\partial z}-\frac{v^2}{r}\right)=-\frac{\partial p}{\partial r}+\frac{\partial \tau_{rr}}{\partial r}+\frac{\partial \tau_{rz}}{\partial z}+\frac{\tau_{rr}-\tau_{\theta\theta}}{r}, \tag{3.2}$$

$$\rho\left(u\frac{\partial v}{\partial r}+w\frac{\partial v}{\partial z}+\frac{uv}{r}\right)=\frac{1}{r^2}\frac{\partial}{\partial r}(r^2\tau_{r\theta})+\frac{\partial \tau_{z\theta}}{\partial z}+\frac{\tau_{r\theta}-\tau_{\theta r}}{r}, \tag{3.3}$$

$$\rho\left(u\frac{\partial w}{\partial r}+w\frac{\partial w}{\partial z}\right)=-\frac{\partial p}{\partial z}+\frac{1}{r}\frac{\partial}{\partial r}(r\tau_{rz})+\frac{\partial \tau_{zz}}{\partial z}, \tag{3.4}$$

Considering no-slip at the disk, one has:

$$u=0, v=r\omega, w=-w_o \;\; at\; z\to 0, \tag{3.5}$$

And fluid velocities vanish outside the boundary layer, so we have:

$$u\to 0, v\to 0 \;\; as\; z\to\infty. \tag{3.6}$$

Now Cauchy stress tensor for Bingham fluid is given by [31]:

$$\tau_{ij}=\begin{cases}\left(\frac{\tau_y}{\dot\gamma}+\mu_p\right)e_{ij}=\eta(\dot\gamma)e_{ij} & \text{for } \tau\geq\tau_y,\\ 0 & \text{for } \tau<\tau_y,\end{cases} \tag{3.7}$$

where $\dot\gamma=(1/2\; e_{ij}e_{ji})^{1/2}$ is the second invariant of the deformation rate tensor in which the terms $e_{ij}=(\partial u_i/\partial x_j+\partial u_j/\partial x_i)$ are components of the strain rate tensor.

Through Eq. (3.7), the components of stress tensor τ are expressed below:

$$\begin{gathered}\tau_{rr}=\eta\left(2\frac{\partial u}{\partial r}\right);\; \tau_{\theta\theta}=\eta\left(2\frac{u}{r}\right);\; \tau_{zz}=\eta\left(2\frac{\partial w}{\partial z}\right);\\ \tau_{r\theta}=\eta\left\{r\frac{\partial}{\partial r}\left(\frac{v}{r}\right)\right\};\; \tau_{\theta z}=\eta\left(\frac{\partial v}{\partial z}\right);\; \tau_{rz}=\eta\left(\frac{\partial u}{\partial z}+\frac{\partial w}{\partial r}\right),\end{gathered} \tag{3.8}$$

And apparent viscosity $\eta(\dot\gamma)$ has the form:

$$\eta(r,z)=\mu_p+\frac{\tau_y}{\sqrt{2\left(\frac{\partial u}{\partial r}\right)^2+2\left(\frac{u}{r}\right)^2+2\left(\frac{\partial w}{\partial z}\right)^2+\left[r\frac{\partial}{\partial r}\left(\frac{v}{r}\right)\right]^2+\left(\frac{\partial v}{\partial z}\right)^2+\left(\frac{\partial u}{\partial z}+\frac{\partial w}{\partial r}\right)^2}}, \tag{3.9}$$

By making use of von-Kármán transformations

$$\zeta=\frac{z}{\sqrt{\nu_p/\omega}}, \tag{3.10}$$

$$(u,v,w)=\left(r\omega F(\zeta),r\omega G(\zeta),H(\zeta)\sqrt{\nu_p\omega},\right), \tag{3.11}$$

$$(p,T)=\left(p_\infty-\omega\mu P(\zeta),T_\infty+(T_w-T_\infty)\theta(\zeta)\right),$$

where ζ is the dimensionless distance that is measured along the rotation axis, the respective equations transform into the following locally similar equations:

$$2F+H'=0, \tag{3.12}$$

$$\begin{aligned}F^2-G^2+HF'&\\ =\left(1+\frac{Bn}{\Lambda}\right)F''-\frac{2Bn}{\Lambda^3}F(G'^2+F'^2)&\\ -\frac{Bn}{2\,\Lambda^3}F'\left[8FF'+4H'H''+2r^{*2}Re(G'G''+F'F'')\right],&\end{aligned} \tag{3.13}$$

$$2FG+HG'=\left(1+\frac{Bn}{\Lambda}\right)G''-\frac{Bn}{2\,\Lambda^3}G'\left[8FF'+4H'H''+2r^{*2}Re(G'G''+F'F'')\right], \tag{3.14}$$

where $\Lambda\equiv\sqrt{4F^2+2H'^2+Re[r^{*2}(G'^2+F'^2)]}$.

And the boundary conditions transform into the following forms:

$$F(0)=0,G(0)=1,H(0)=-A \text{ as } \zeta\to 0, \tag{3.15}$$

$$F\to 0\ ,G\to 0 \text{ as } \zeta\to\infty. \tag{3.16}$$

In Eqs. (3.13)- (3.16), $A=w_o/\sqrt{rw}$ is the wall suction parameter, $Bn=\tau_y/\mu_p\omega$ denotes the Bingham number and $Re=R^2\omega/\nu_p$ represents the Reynolds number for disk of radius R.

3.2.1 Heat transfer analysis

Heat transfer takes place as a result of difference in temperature at the disk surface and that of the fluid at infinity. In presence of viscous dissipation, the energy equation can be expressed in the form:

$$\rho c_p \left(u \frac{\partial T}{\partial r} + w \frac{\partial T}{\partial z} \right) = k \nabla^2 T + \Phi, \tag{3.17}$$

where k stands for thermal conductivity, c_p for the specific heat capacity and Φrepresents the viscous dissipation term given below:

$$\Phi = \tau_{rr} \left(\frac{\partial u}{\partial r} \right) + \tau_{\theta\theta} \left(\frac{u}{r} \right) + \tau_{zz} \left(\frac{\partial w}{\partial z} \right) + \tau_{r\theta} \left[r \frac{\partial}{\partial r} \left(\frac{v}{r} \right) \right] + \tau_{rz} \left(\frac{\partial u}{\partial z} + \frac{\partial w}{\partial r} \right) + \tau_{\theta z} \left(\frac{\partial v}{\partial z} \right). \tag{3.18}$$

By using $\theta(\zeta) = (T - T_\infty)/(T_w - T_\infty)$ together with the von-Kármán transformations, equation (3.17) becomes,

$$\frac{1}{Pr} \theta'' - H\theta' + \frac{Ec}{Re} (\wedge + Bn) \wedge = 0. \tag{3.19}$$

Here $Pr = \mu c_p / k$ denotes the Prandtl number and $Ec = R^2 \omega^2 / C_p \Delta T$ is the Eckert number. Eq. (3.19) is to be solved by the conditions:

$$\theta(0) = 1 \quad \text{and} \quad \theta(\infty) = 0. \tag{3.20}$$

3.2.2 Skin friction coefficient, Nusselt number and volumetric flow rate

Quantities of engineering interest are the skin friction coefficient C_f:

$$C_f = \frac{\sqrt{\tau_r^2 + \tau_\varphi^2}}{\rho (r\omega)^2}, \tag{3.21}$$

where τ_r and τ_ϕ denote the radial and azimuthal wall stresses respectively which can be evaluated from Eq. (3.8). Eq. (3.21) in view of transformations [31] becomes:

$$r^* C_f = \frac{Bn}{Re} + \left\{ \frac{(F'(0))^2 + \left(G'(0)\right)^2}{Re} \right\}^{1/2}. \tag{3.22}$$

Nusselt number Nu measuring the importance of convective heat transfer relative to conductive heat transfer is defined as follows:

$$Nu = \frac{L q_w}{k(T_w - T_\infty)}, \tag{3.23}$$

where q_w denotes the wall heat flux. Using the length scale L as $\sqrt{\nu_p/\omega}$, Eq. (3.23) reduces to:

$$Nu = -\theta'(0). \tag{3.24}$$

The pumping efficiency of the finite disk can be computed using the following definite integral [16];

$$Q = \int_0^{r_o} -w(\infty)2\pi r\,dr = -H(\infty)\pi\sqrt{\nu\omega}\,r_o^2. \tag{3.25}$$

3.2.3 Entropy generation equation

The entropy generation rate is defined as follows (see Lopez et al. [36], Hayat et al. [37], Rashidi et al. [38], etc.):

$$\dot{S}'''_{gen} = \frac{k}{T_\infty^2}\left[\left(\frac{\partial T}{\partial r}\right)^2 + \left(\frac{1}{r}\frac{\partial T}{\partial \theta}\right)^2 + \left(\frac{\partial T}{\partial z}\right)^2\right] + \frac{\Phi}{T_\infty}, \tag{3.26}$$

First part of Eq. (3.26) signifies the entropy production due to thermal irreversibility and second part corresponds to the fluid friction irreversibility.

The dimensionless form of the entropy generation rate is the entropy generation number N_G which is the ratio of the actual entropy generation rate $\dot{S}'''$ to the characteristic entropy generation rate $\dot{S}_0$. It is evaluated as follows:

$$N_G = \dot{S}'''_{gen}/(k\omega\Delta T/\nu T_\infty) = \alpha\theta'^2 + \frac{Pr.Ec}{Re}(\wedge + Bn)\wedge, \tag{3.27}$$

where $\alpha = \Delta T/T_\infty$ measures the wall and ambient temperature difference

3.3 Numerical Method

The normalized velocity and temperature profiles are computed from the equations (3.13)-(3.16), (3.19) and (3.20) by means of MATLAB routine bvp4c based on collocation formula. First we convert the equations (3.13)-(3.16), (3.19) and (3.20) into first order by substituting:

$$Y_1 = F; Y_2 = F'; Y_3 = G; Y_4 = G'; Y_5 = H; Y_6 = \theta; Y_7 = \theta', \tag{3.28}$$

We obtain the following system (see Sadeghy et al. [31]):

$$Y_1' = Y_2; \tag{3.29}$$

$$Y_2' = \frac{1}{K_1[K_2K_3(Y_4^2 + Y_2^2) - K_1]}\,[2K_2(K_2Y_4^2K_3 - K_1)Y_1(Y_4^2 + Y_2^2) \tag{3.30}$$

$$+K_2K_3(Y_1^2 - Y_3^2)Y_4^2 - 2K_2K_3Y_1Y_2Y_3Y_4 + 4K_1(-3K_2Y_2^2Y_1 + \frac{Y_3^2 - Y_1^2}{4} - \frac{1}{4}Y_5Y_2)];$$

$$Y_3' = Y_4; \tag{3.31}$$

$$Y_4' = \frac{1}{K_1[K_2K_3(Y_4^2 + Y_2^2) - K_1]}[-2K_3Y_4Y_2Y_1(Y_4^2 + Y_2^2)K_2^2 + Y_4\{-8K_2K_1Y_1Y_2 \tag{3.32}$$

$$-K_2\big(-Y_3^2K_3 + Y_1(K_3Y_1 + 4K_1)\big)Y_2 - Y_5K_1\} + 2Y_1Y_3(K_2K_3Y_2^2 - K_1)];$$

$$Y_5' = -2Y_1; \tag{3.33}$$

$$Y_6' = Y_7; \tag{3.34}$$

$$Y_7' = \Pr\left[Y_5Y_7 - \frac{Ec}{Re}(\wedge + Bn)\wedge\right]; \tag{3.35}$$

whereK_1, K_2 and K_3stands for:

$$K_1 = \left(1 + \frac{Bn}{\wedge}\right), K_2 = \frac{Bn}{\wedge^3}, K_3 = r^{*2}Re, \tag{3.36}$$

It should be remarked here that the above system with the exception of energy equation were presented by Sadeghy et al. [31].

3.4 Results and discussion

Heat transfer to swirling flow of Bingham fluids along a rotating disk is modeled here. Following Sadeghy et al. [31], numerical integrations are carried out at $r^\star = 1$, that is, at the rim of the disk for certain range of embedded parameters which include Eckert number Ec, Prandtl number Pr, Bingham number Bn and wall suction parameter A. Table 3.1 displays the numerical results of wall skin friction $r^\star C_f$ at different values of Bingham number Bn. Since apparent viscosity in the present problem is given by the factor $(1 + Bn/\wedge)$ so we predict that skin friction coefficient should elevate as parameter Bn enlarges. Physically a growth in Bn implies an elevation in fluid

yield stress (τ_y) which in turn results in higher resisting torque at the disk surface. In Table 3.2, local Nusselt number data is presented by varying the parameters $Bn, \Pr$ and Ec. Note that by increasing fluid yield stress (τ_y), heat transfer through the disk deteriorates significantly. As Prandtl number enlarges, the relative importance of momentum diffusion increases due to which local Nusselt number enlarges. Furthermore, it is predicted that by increasing the intensity of viscous dissipation the rate of heat transfer from the solid surface should decrease.

The behavior of Bingham number Bn on all three velocities (u, v, w) and temperature profile θ is portrayed through Figs. 3.1a-3.1d at a specific parameter value $A = 1$. Fig. 3.1a depicts that radially outward flow caused by centrifugal force decelerates throughout the boundary layer by increasing fluid yield stress. Maximum radial velocity is attained at a higher axial distance as parameter Bn enlarges. Fig. 3.1b displays the azimuthal velocity curves, represented by $G(\zeta)$, for various values of Bn. It is clear that circumferential velocity grows and boundary layer expands where fluid yield stress is enhanced. The reduction in radial fluid motion upon increasing Bn (as clarified in Fig. 3.1a) must be compensated by a decrease in downward axial velocity (see Fig. 3.1c). In other words, the pumping efficiency of the disk, that depends on absolute value of $H(\infty)$, is much reduced in the presence of yield stress. Physically the amount of fluid sucked from a region of lower temperature to a region of higher temperature decreases with increasing Bn. As a consequence, thermal boundary layer appears to expand upon increasing fluid yield stress (see Fig. 3.1d). Temperature curves become thick as Bn becomes large signaling a reduction in wall temperature gradient.

In Figs. 3.2a-3.2d, velocity and temperature curves as functions of dimensionless axial coordinate ζ are plotted for a variety of wall suction parameters. In existence of wall suction, radial velocity is decreasing compared with the case of no suction velocity (see Fig. 3.2a). The permeable nature of the disk also gives opposition to the induced azimuthal flow near the disk as clear from Fig. 3.2b. Dissimilar to the effect of Bingham number Bn, the amount of fluid drawn in the axial direction grows as wall suction becomes strong. It was shown by Turkyilmazoglu and Senel [11], via asymptotic expressions, that the axial velocity component becomes constant when sufficiently large suction velocity is imposed. The same tendency appears here since profile of H transforms into a straight line as parameter A increases. Consequently, thermal

boundary layer suppresses with increasing A and magnitude of this decrease in θ becomes zero for sufficiently large values of A.

Figs. 3.3a and 3.3b demonstrate the behaviors of Prandtl numberPr and Eckert number Ec on temperature profile respectively. In Fig. 3.3a, the thermal boundary layer suppress by increasing Pr. This is because the importance of thermal diffusion compared to momentum diffusion reduces with increasing Pr. Also, temperature profile becomes steeper when higher Pr is considered. This signals a growth in the value of local Nusselt number. Furthermore, by increasing Eckert number Ec, heat generation due to fluid friction enhances at a given temperature gradient. This in turn leads to thicker temperature profiles as anticipated.

Figs. 3.4a-3.4c display the wall skin friction $r^{\star}C_f$, local Nusselt number Nu and dimensionless volumetric flow rate $-H(\infty)$ as functions of Bingham number Bn. Computations are made at several values of wall suction parameter A. Eq. (3.22) shows that $r^{\star}C_f$ has a direct relation with Bingham number Bn. It is further clarified via Figs. 3.1a and 3.1b that wall velocity gradients $F'(0)$ and $G'(0)$ are decreasing functions of Bn. Due to these reasons, a decreasing trend in skin friction coefficient becomes apparent when Bn is incremented. Although, local Nusselt number is marginally influenced by Bingham number but it is significantly enhanced as wall suction gets strong. Fig. 3.4c shows that far field axial flow accelerates upon increasing wall suction parameter A. It should be noted that variation in $H(\infty)$ with Bn becomes smaller as parameter A gradually increases. Eventually, the graph of $H(\infty)$ versus Bn becomes a straight line in case of strong wall suction.

Entropy generation number N_G is a useful tool to predict spatial variation in entropy production across the boundary layer. Figs. 3.5a-3.5d plot the behaviors of different parameters on N_G. It appears that entropy production rate is maximum at the disk and it gradually decreases with increasing axial distance. A cross-over in N_G profiles is apparent in Fig. 3.5a illustrating that entropy generation decreases near the disk and increases near the edge of boundary layer when fluid's yield stress is enhanced. Fig. 3.5b elucidates that the impact of Prandtl number is to enhance the entropy production throughout the boundary layer. According to Fig. 3.5c, the entropy generation rate is much enhanced when viscous dissipation effect is present. Fig. 3.5d depicts that higher the fluid yield stress, greater is the entropy production within the von-Kármán's boundary layer.

Table 3.1: Effect of Bingham number Bn, on skin friction coefficient $r^{\star}C_f$ when $r^{*} = 1, Re = 2950$ and $A = 1$.

Bn	$F'(0)$	$G'(0)$	$r^{\star}C_f$
0	0.38956	-1.17522	0.02279
10	0.32344	-1.13896	0.02519
20	0.27708	-1.11538	0.02794
30	0.24208	-1.09859	0.03088
50	0.19274	-1.07631	0.03708

Table 3.2: Effect of Bingham number Bn, Prandtl number Pr and Eckert number Ec on $\theta'(0)$ when $r^{*} = 1, Re = 2950$ and $A = 1$.

Bn	Pr	Ec	$\theta'(0)$
0	5	0.2	-4.47919
10	5	0.2	-4.31126
20	5	0.2	-4.13891
30	5	0.2	-3.96382
50	5	0.2	-3.60851
10	2	0.2	-1.77831
10	3	0.2	-2.62405
10	5	0.2	-4.31126
10	7	0.2	-5.99953
10	5	0	-5.06572
10	5	0.2	-4.31126
10	5	0.4	-3.55681
10	5	0.6	-2.80235

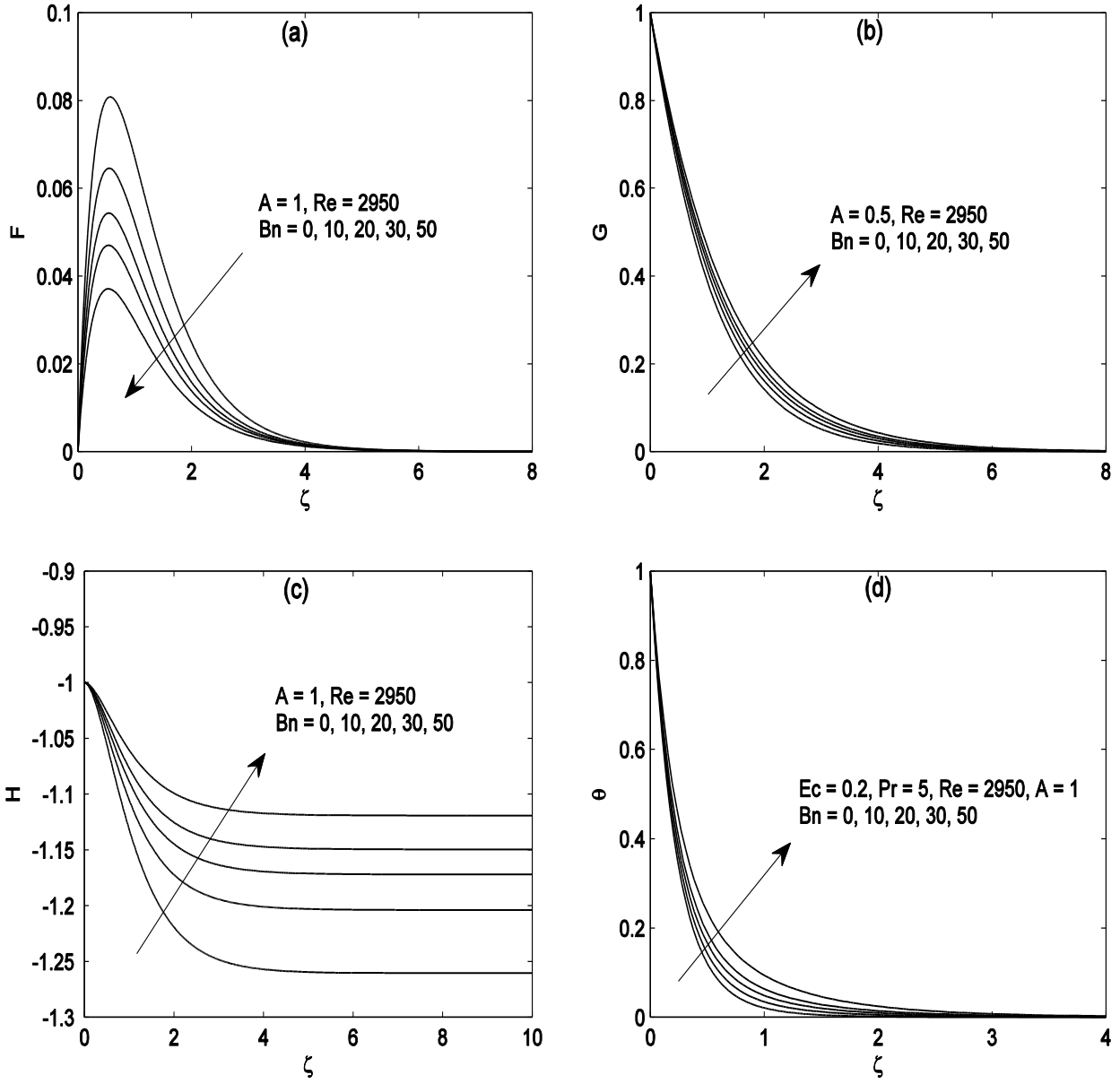

Fig. 3.1: Variation in normalized velocity components (F, G, H) and temperature (θ) with ζ at different values of Bingham number Bn.

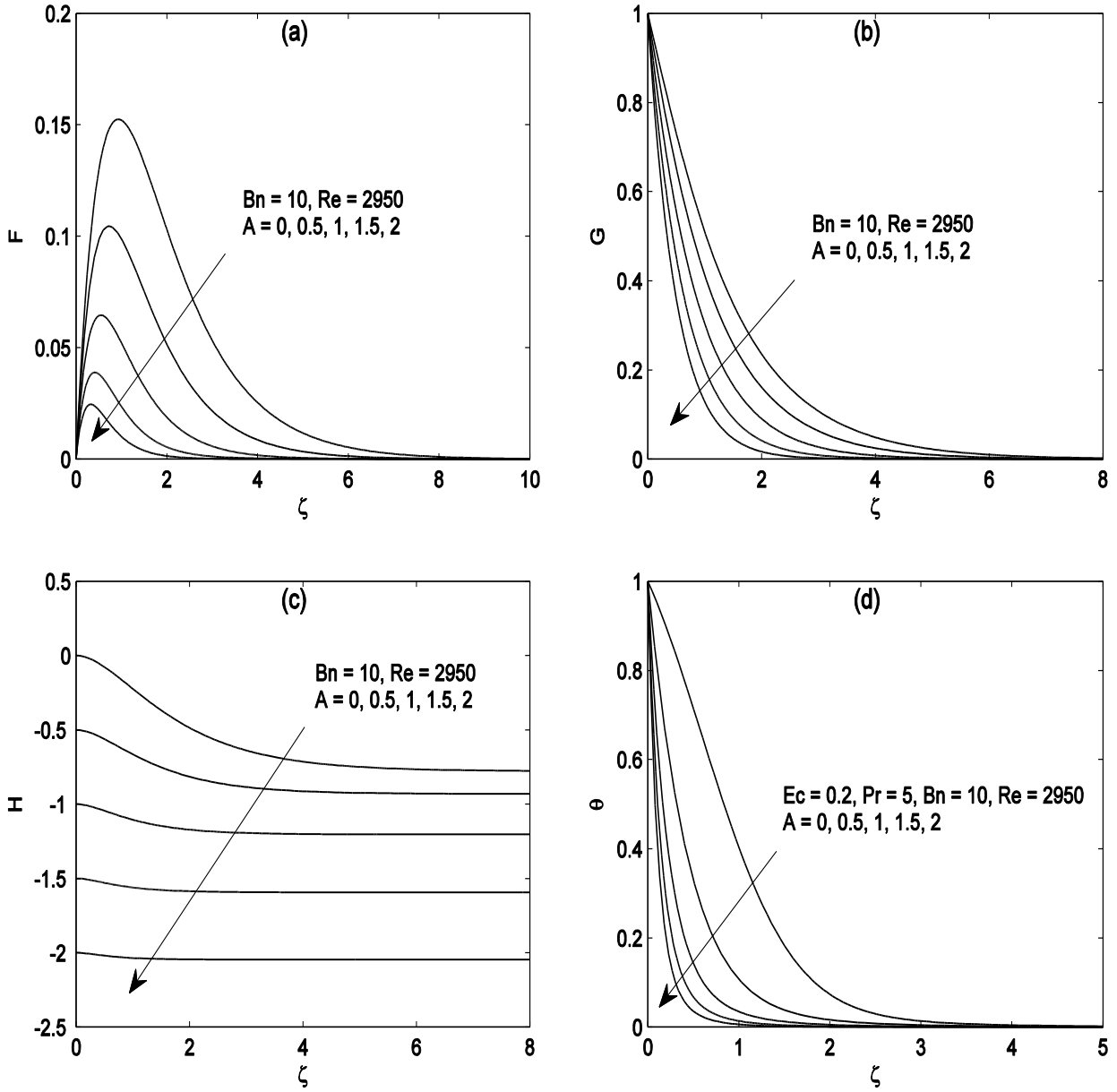

Fig. 3.2: Variation in normalized velocity components (F, G, H) and temperature (θ) with ζ for various values of wall suction parameter A.

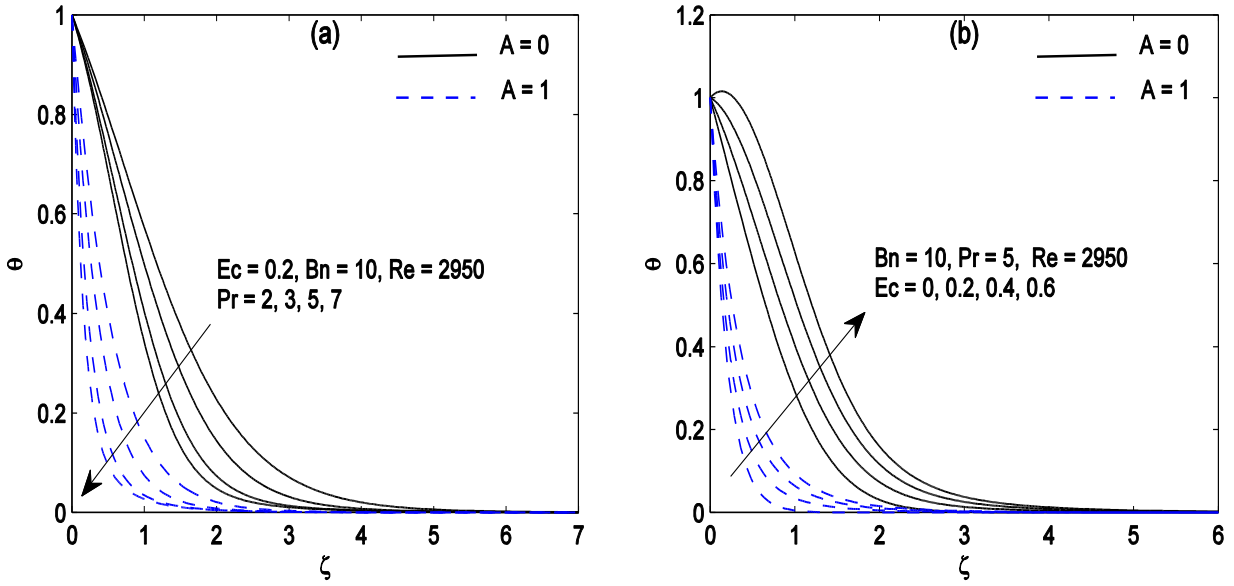

Fig. 3.3: Temperature (θ) profiles with ζ for various values of (a) Prandtl number Pr and (b) Eckert number (Ec).

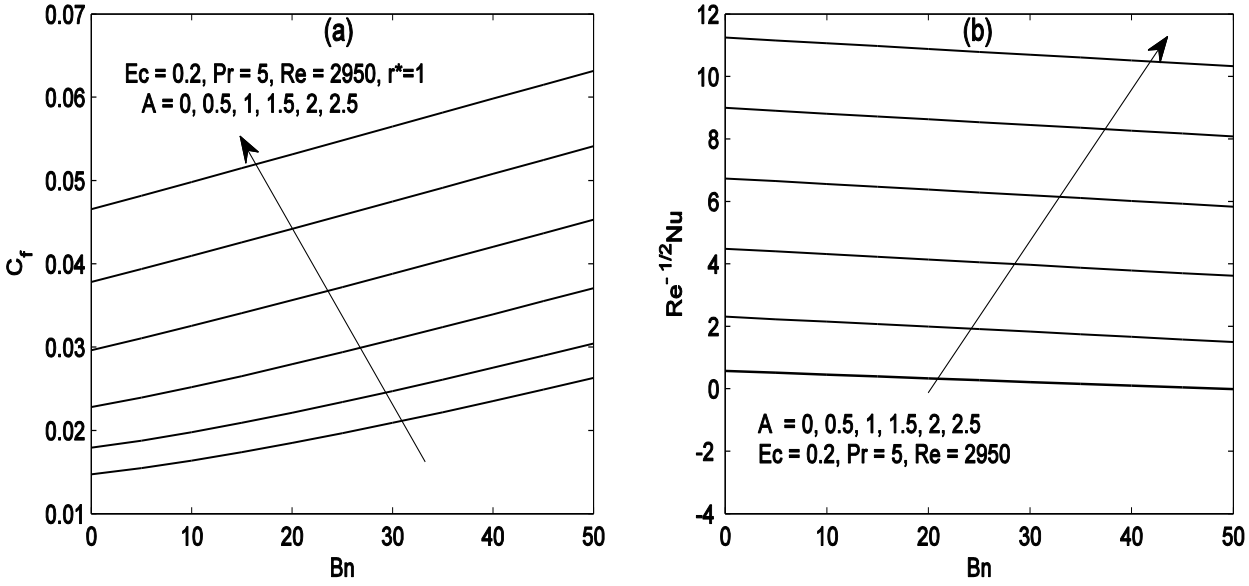

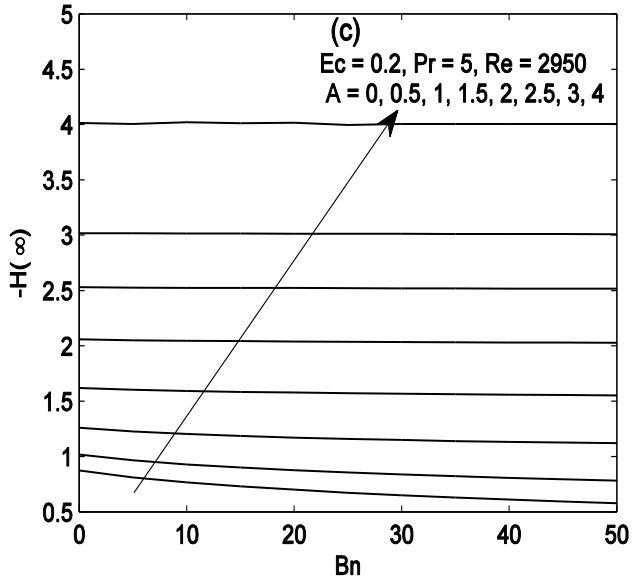

Fig. 3.4: Effect of Bingham number Bn and suction parameter A on (a) skin friction coefficient C_f, (b) local Nusselt number $Re^{-1/2}Nu$ and (c) dimensionless volumetric flow rate $-H(\infty)$.

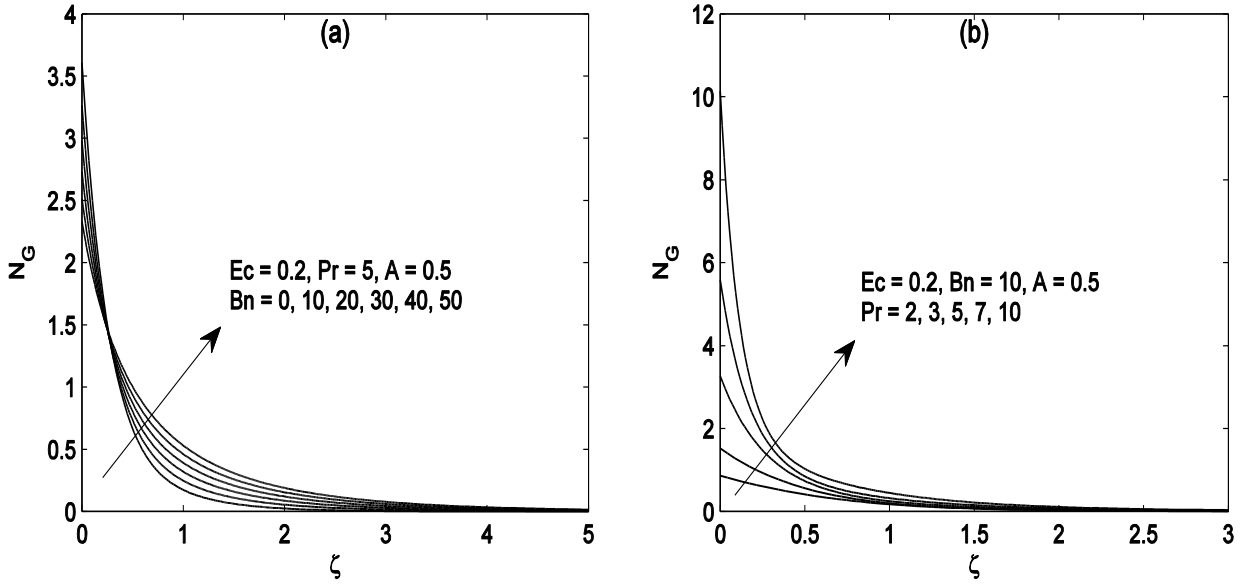

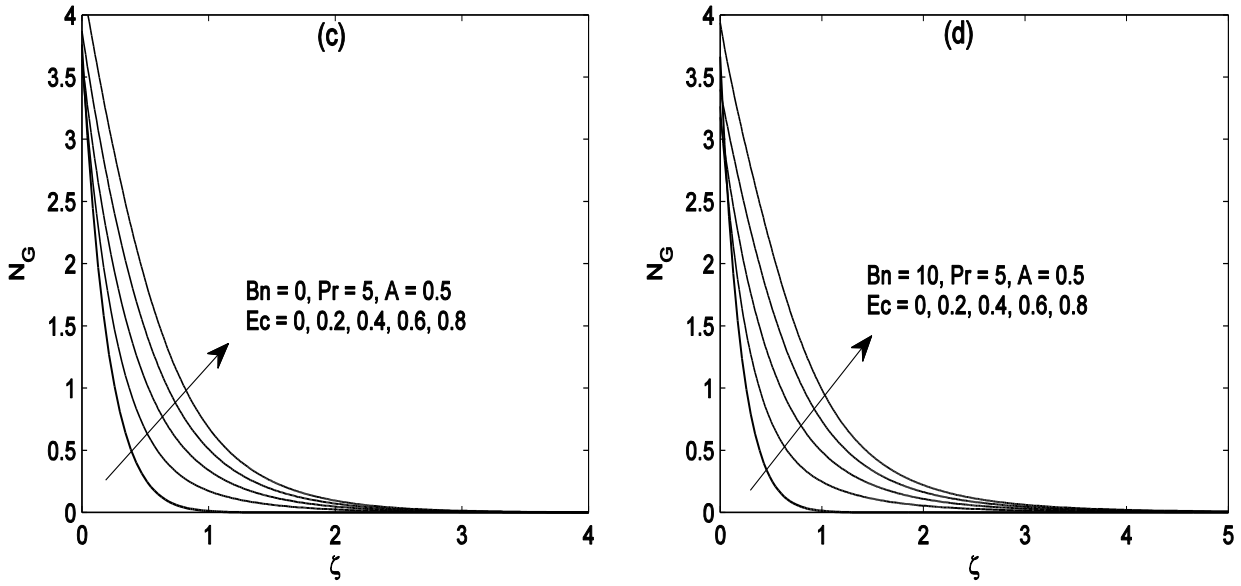

Fig. 3.5: Results of entropy generation number N_G with ζ for different values of embedded parameters when $\alpha = 0.5$.

3.5 Concluding remarks

An analysis is carried out for heat transfer in von-Kármán flow of Bingham fluid subject to wall suction. A similarity solution is achieved that enabled us to discover the role of yield stress on heat transfer and entropy generation rate. On the basis of present analysis, following observations are made:

i. The retarding effect of fluid suction on the radial and azimuthal velocities is apparent from the numerical results.

ii. Axial velocity profile becomes constant as the wall suction effect enlarges. Furthermore, there is no variation in entrainment velocity $H(\infty)$ with Bingham number Bn for strong wall suction.

iii. Inclusion of wall suction phenomenon leads to an enhancement in the amount of cold fluid that is drawn towards the disk. This results in the thinning of thermal boundary layer and growth in wall heat transfer rate.

iv. The variation in solution profiles with increasing Bingham number reduces in magnitude when fluid is sucked at a higher velocity.

v. Heat penetration depth grows upon increasing fluid yield stress. This effect accompanies with lower heat transfer rate from solid surface.

vi. Entropy generation rate decreases monotonically with increasing vertical distance and asymptotes to zero value.

vii. The presence of yield stress has led to a growth in entropy generation rate within the boundary layer.

References

1. T. von Kármán, Überlaminare und turbulenteReibung, Zeitschrift fur Angew. Math. Mech. ZAMM 1 (1921) 233-252.
2. W. G. Cochran, The flow due to a rotating disk, Proceedings of the Cambridge Philosophical Society 30 (1934) 365–375.
3. K. Millsaps and K. Pohlhausen, Heat transfer by laminar flow from a rotating disk, J. Aeronaut. Sci. 19 (1952) 120–126.
4. J. A. D. Ackroyd, On the steady flow produced by a rotating disk with either surface suction or injection, Journal of Engineering Mathematics 12 (1978) 207–220.
5. G. K. Batchelor, Note on the class of solutions of the Navier–Stokes equations representing steady non-rotationally symmetric flow, Quart. J. Appl. Math. 4 (1951) 29-41.
6. U. T. Bödewadt, Die DrehströmungüberfestemGrund, Z. angew Math. Mech. 20 (1940) 241-252.
7. P. J. Zandbergen and D. Dijkstra, Von Kármán swirling flows, Ann. Rev. Fluid Mech. 19 (1987) 465-491.
8. M. Miclavcic and C. Y. Wang, The flow due to a rough rotating disk, Z. angew. Math. Phys. 54 (2004) 1-12.
9. S. S. Chawla, P. K. Srivastava and A. S. Gupta, Rotationally symmetric flow over a rotating disk, Int. J. Non-Linear Mech. 44 (2009) 717-726.
10. M. Turkyilmazoglu, Three dimensional MHD stagnation flow due to a stretchable rotating disk, Int. J. Heat & Mass Transf. 55 (2012) 6959-6965.
11. M. Turkyilmazoglu and P. Senel, Heat and mass transfer of the flow due to a rotating rough and porous disk, Int. J. Therm. Sci. 63 (2013) 146-158.
12. T. Hayat, M. Rashid. M. Imtiaz and A. Alsaedi, Magnetohydrodynamic (MHD) flow of Cu-water nanofluid due to a rotating disk with partial slip, AIP Adv. 5 (2015) Article ID 067169; doi: 10.1063/1.4923380.

13. J. A. Khan, M. Mustafa, T. Hayat and A. Alsaedi, A revised model to study the MHD nanofluid flow and heat transfer due to rotating disk: numerical solutions, Neural Comput. &Applicat. (2016); doi: 10.1007/s00521-016-2743-4.
14. I. Mustafa, T. Javed and A. Ghaffari, Heat transfer in MHD stagnation point flow of a ferrofluid over a stretchable rotating disk, J. Molec. Liq. 219 (2016) 526-532.
15. M. Mustafa, MHD nanofluid flow over a rotating disk with partial slip effects: Buongiorno model, Int. J. Heat & Mass Transf. 108 (2017) 1910-1916.
16. H. I. Andersson, E. de Korte and R. Meland, Flow of a power-law fluid over a rotating disk revisited, Fluid Dynam. Res. 28 (2001) 75-88.
17. H. A. Attia, The effect of ion-slip on the flow of Reiner-Rivlin fluid due to a rotating disk with heat transfer, J. Mech. Sci. & Tech. 21 (2007) 174-183.
18. P. T. Griffiths, Flow of a generalised Newtonian fluid due to a rotating disk, J. Non-Newtonian Fluid Mech. 221 (2015) 9-15.
19. S. Xun, J. Zhao, L. Zheng, X. Chen and X. Zhang, Flow and heat transfer of Ostwald-de Waele fluid over a variable thickness rotating disk with index decreasing, Int. J. Heat & Mass Transf. 103 (2016) 1214-1224.
20. D. H. Doh and M. Muthtamilselvan, Thermophoretic particle deposition on magnetohydrodynamic flow of micropolar fluid due to a rotating disk, Int. J. Mech. Sci. 130 (2017) 350-359.
21. C. Ming, L. Zheng, X. Zhang, F. Liu and V. Anh, Flow and heat transfer of power-law fluid over a rotating disk with generalized diffusion, Int. Commun. Heat & Mass Transf. 79 (2016) 81-88.
22. F. Labropulu and D. Li, Stagnation-point flow of a second-grade fluid with slip, Int. J. Non-Linear Mech. 43 (2008) 941-947.
23. M. Reiner, A mathematical theory of dilatancy, Amer. J. Math. Soc. 67 (1945) 350-362.
24. R. S. Rivlin, The hydrodynamics of non-Newtonian fluids , I, Proc. R. Soc. London A 193 (1948) 260-281.

25. L. Zheng, Y. Li and X. Zhang, Slip effects on MHD flow of a generalized Oldroyd-B fluid with fractional derivative, Nonlinear Anal. Real World Appl. 13 (2012) 513-523.
26. B. Sahoo and S. Poncet, Flow and heat transfer of a third grade fluid past an exponentially stretching sheet with partial slip boundary condition, Int. J. Heat & Mass Transf. 54 (2011) 5010-5019.
27. T. Javed and I. Mustafa, Slip effects on a mixed convection flow of a third-grade fluid near the orthogonal stagnation point on a vertical surface, J. Appl. Mech. Tech. Phys. 57 (2016) 527-536.
28. D. S. Chauhan and A. Olkha, Slip flow and heat transfer of a second-grade fluid in a porous medium over a stretching sheet with power-law surface temperature or heat flux, Chem. Eng. Commun. 198 (2011) 1129-1145.
29. S. Hina, M. Mustafa, T. Hayat and A. Alsaedi, Peristaltic flow of Powell-Eyring fluid in curved channel with heat transfer: A useful application in biomedicine, Comp. Meth. &Prog. Biomed. 135 (2016) 89-100.
30. S. Abbasbandy, M. Mustafa, T. Hayat and A. Alsaedi, Slip effects on MHD boundary layer flow of Oldroyd-B fluid past a stretching sheet: An analytic solution, J. Brazilian Soc. Mech. Sci. Eng. 39 (2017) 3389-3397.
31. A. Ahmadpour and K. Sadeghy, Swirling flow of Bingham fluids above a rotating disk: An exact solution, J. Non-Newtonian Fluid Mech. 197 (2013) 41-47.
32. M. Turkyilmazoglu, Nanofluid flow and heat transfer due to a rotating disk. Comput. & Fluids 94 (2014) 139-146.
33. M. M. Rashidi, S. A. M. Pour, T. Hayat and S. Obaidat, Analytic approximate solutions for steady flow over a rotating disk in porous medium with heat transfer by homotopy analysis method, Comput. & Fluids 54 (2012) 1-9.
34. A. Guha and S. Sengupta, Analysis of von Kármán's swirling flow on a rotating disc in Bingham fluids, Phys. Fluids 28 (2016) Article ID 013601, doi: https://doi.org/10.1063/1.4937590.

35. M. Tabassum and M. Mustafa, A numerical treatment for partial slip flow and heat transfer of non-Newtonian Reiner-Rivlin fluid due to rotating disk, Int. J. Heat & Mass Transf. 123 (2018) 979-987.
36. A. Lopez, G. Ibanez, J. Pantoja, J. Moreira and O. Lastres, Entropy generation analysis of MHD nanofluid flow in a porous vertical microchannel with nonlinear thermal radiation, slip flow and convective-radiative boundary conditions, Int. J. Heat & Mass Transf. 107 (2017) 982-994.
37. T. Hayat, S. Qayyum, M. I. Khan and A. Alsaedi, Entropy generation in magneto-hydrodynamic radiative flow due to rotating disk in presence of viscous dissipation and Joule heating, Phys. Fluids 30 (2018), Article ID 017101; doi: https://doi.org/10.1063/1.5009611.
38. M. M. Rashidi, S. Abelman and N. FreidooniMehr, Entropy generation in steady MHD flow due to a rotating porous disk in a nanofluid, Int. J. Heat & Mass Transf. 62 (2013) 515-525.
39. Lawrence F. Shampine, Jacek Kierzenka and Mark W. Reichelt, Solving boundary value problems for ordinary differential equations in matlab with bvp4c,CEM-UVM, (2000).